

# HYDRO-GEOTECHNICAL ASSESSMENT OF SCOUR OF ROCK

Dr Steven Pells<sup>1</sup>; Dr Kurt Douglas<sup>2</sup>.

1. Principal, PSM
2. UNSW Sydney

Spillways for dams are commonly lined with concrete to control the flow of water and to offer resistance to scour / erosion<sup>1</sup>. Despite this, for practical or economic reasons, many spillways may be left unlined where the local rock mass is judged to be sufficiently resistant to scour. Erosion within the spillway can incur expensive repair or even create a risk of dam failure. Proper assessment of the potential for scour of rock masses must give equal weight to hydraulic and geotechnical factors. In this paper, a methodology for hydro-geotechnical assessment of scour in rock is presented, to guide this multi-disciplinary assessment. The methodology has been formed following review of over 30 case studies of spillway scour, and with consideration to current best-practice techniques in both rock-mechanics and hydraulics. Emerging technologies and further research that will improve the capacity to predict scour are identified to guide future research and development.

## Introduction

The risk from erosion is a key matter of consideration when designing new spillways. Also, for existing spillways, the risk of erosion may be reviewed as part of routine surveillance, or if changes to the dam arrangement or design flood conditions are being considered. It may also be necessary to assess scour damage that has already occurred. For large dams, an unlined section would only be considered where relatively competent rock exists. This risk assessment process therefore typically requires an assessment of erosion of rock masses to be made.

Erosion of rock masses is dissimilar to erosion of earth or soil. Typically, the rock substance remains intact, but structural features of rock masses (i.e. defects within the rock-mass) create distinct but interlocking units of rock, which may be unraveled by hydraulic forces. Assessment of erosion of rock masses therefore requires a multi-discipline approach, applying expertise in both rock mechanics and hydraulics. Such an assessment has been termed herein as a "hydro-geotechnical rock scour assessment".

Multi-discipline engineering can suffer from misunderstanding and miscommunication. In this paper, a methodology to guide the undertaking of a hydro-geotechnical rock scour assessment is presented. Descriptions of the individual tasks are given with reference to current best-practice in both rock-mechanics and hydraulics. Emerging technologies and new research which will assist with rock-scour assessments are also identified to guide future research and development.

---

<sup>1</sup> The terms 'scour' and 'erosion' are considered synonymous for the purpose of this paper.

## Methodology for erosion assessment

A “hydro-geotechnical rock scour assessment” is considered to conform to the flowchart presented in Figure 1 below. Each of the steps (1. to 8.) in the flowchart are discussed in turn below.

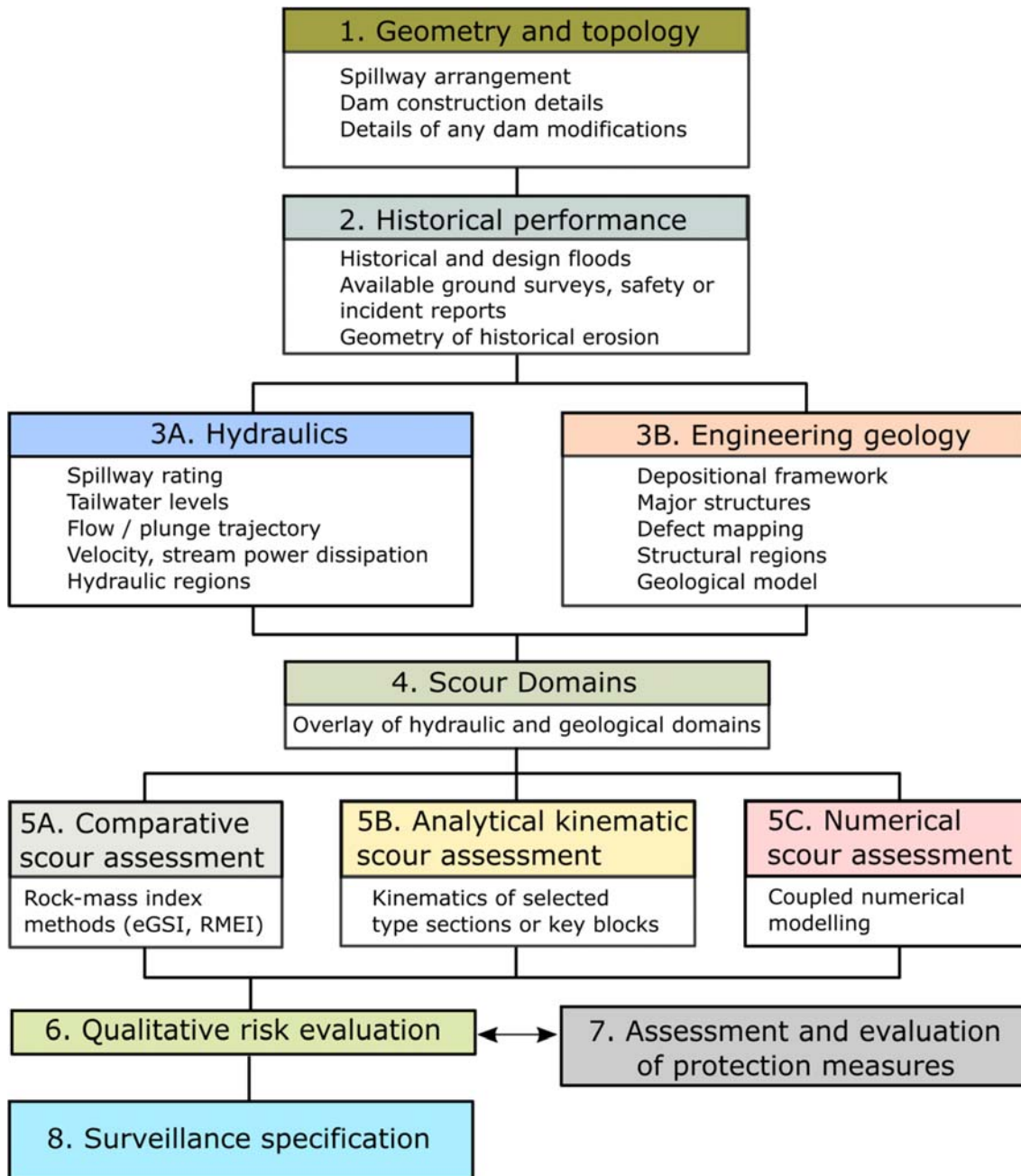


Figure 1 – Flowchart for hydro-geotechnical assessment of erosion of unlined spillways

## 1. Geometry and topology

In assessment of spillway scour, the entire spillway is usually considered, extending from the reservoir through to a location on the natural river bed downstream of the spillway where flow conditions are returning to their natural (pre-dam) condition (Figure 2). The topography of this entire region must be compiled and presented in maps, with reference to available ground-survey data and dam design or as-constructed drawings. It is recommended that 3D representations of the geometry are constructed (e.g. Figure 3) as this communicates a clear perspective of the problem.

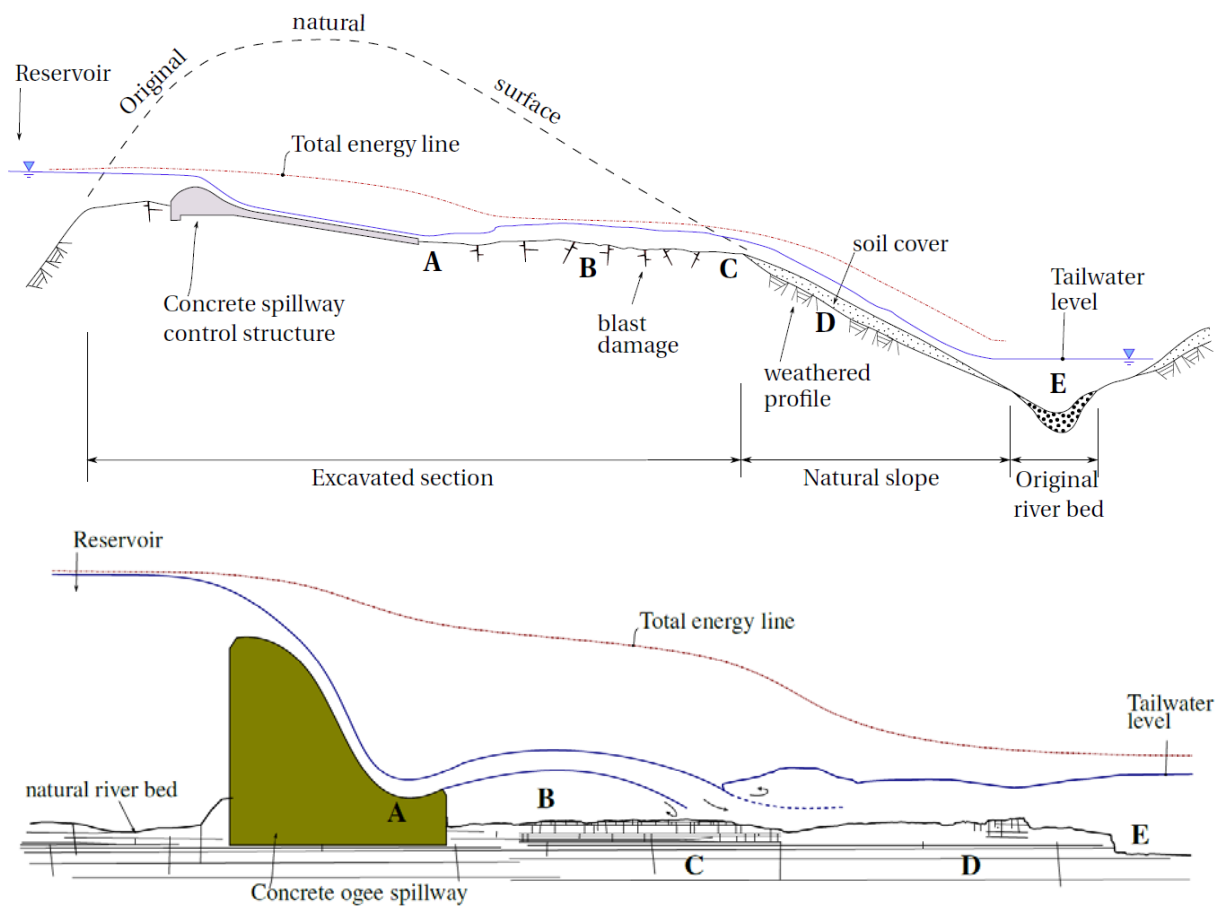


Figure 2 – Examples of the region of assessment for typical side-channel spillways (top) and concrete gravity ogee spillways (bottom)

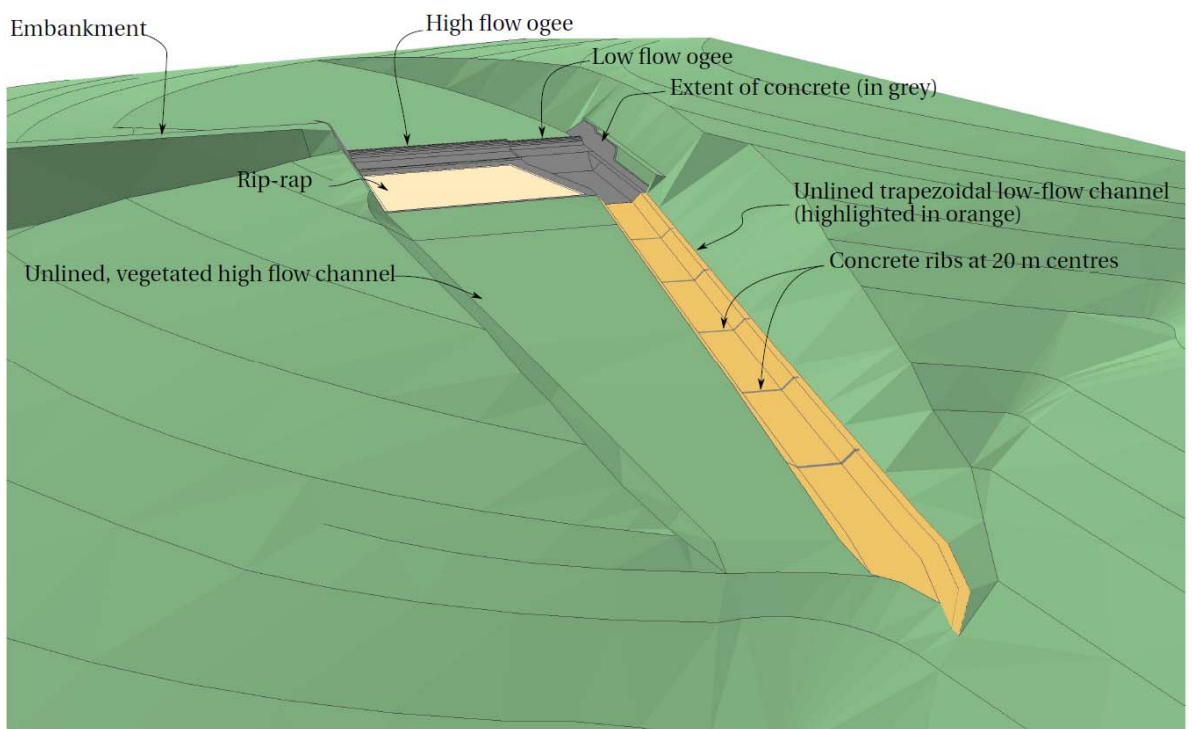
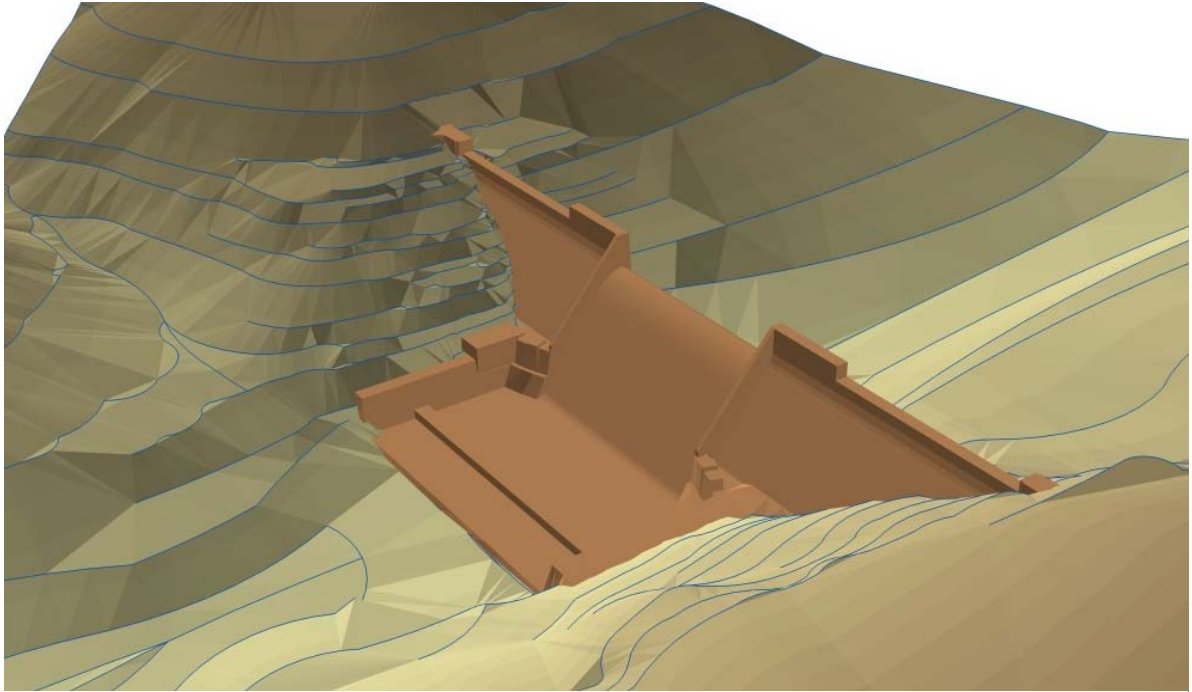


Figure 3– Examples of 3D representations of dam spillway topology

## 2. Historical performance

Where historical erosion has occurred, detailed ground surveys, ideally successive, should be obtained to allow examination of the extent and form of erosion (e.g. Figure 4).

The available information on design flood conditions should be obtained. For existing dams, a record of historical spills should be compiled and should be related to the available topographic data, correlating any historical erosion with past events. Where recorded reservoir levels are available, it is recommended to plot data as a timeseries, showing crest elevations of spillway inlets or overflow points (e.g. Figure 5).

Historical photographs of the dam should also be compiled, including photographs of the rock mass during previous inspections or during construction and any available photographs of the spillway in operation.

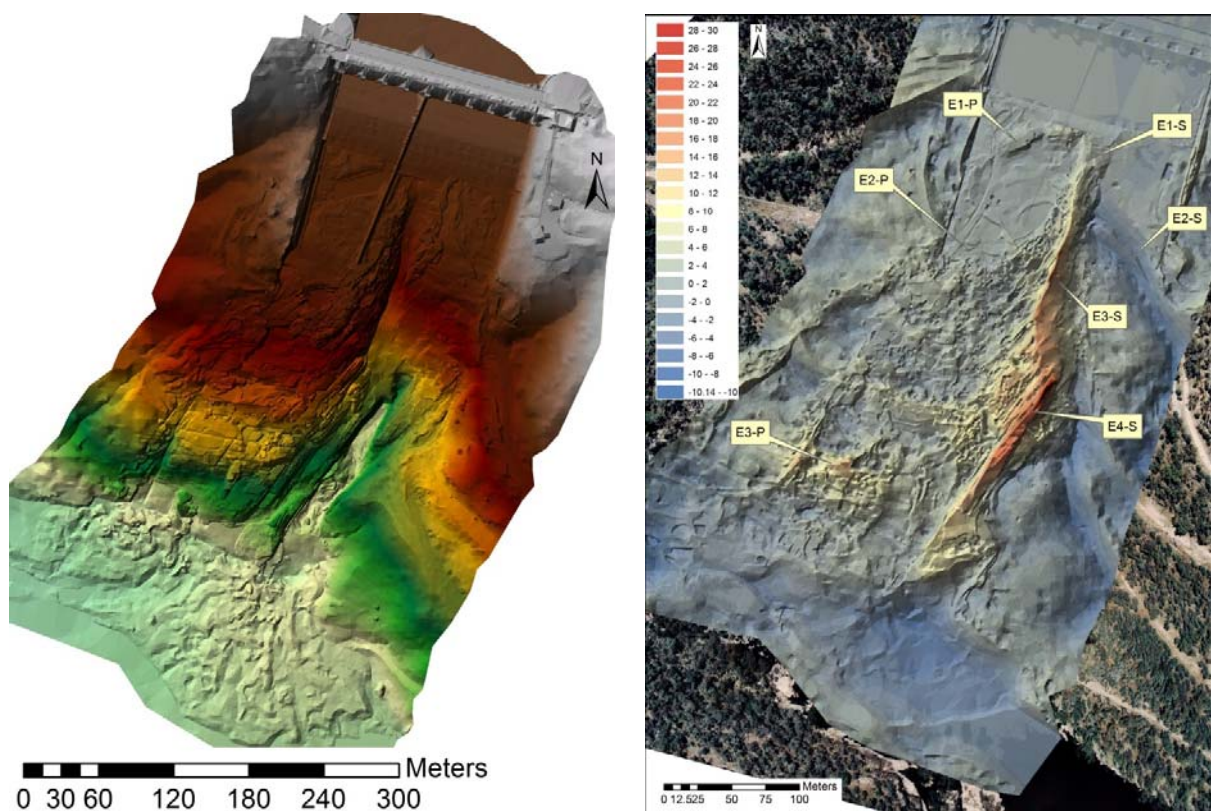


Figure 4 – Examples of representations of historical erosion showing topography (left) and isopachs of erosion depth (right)

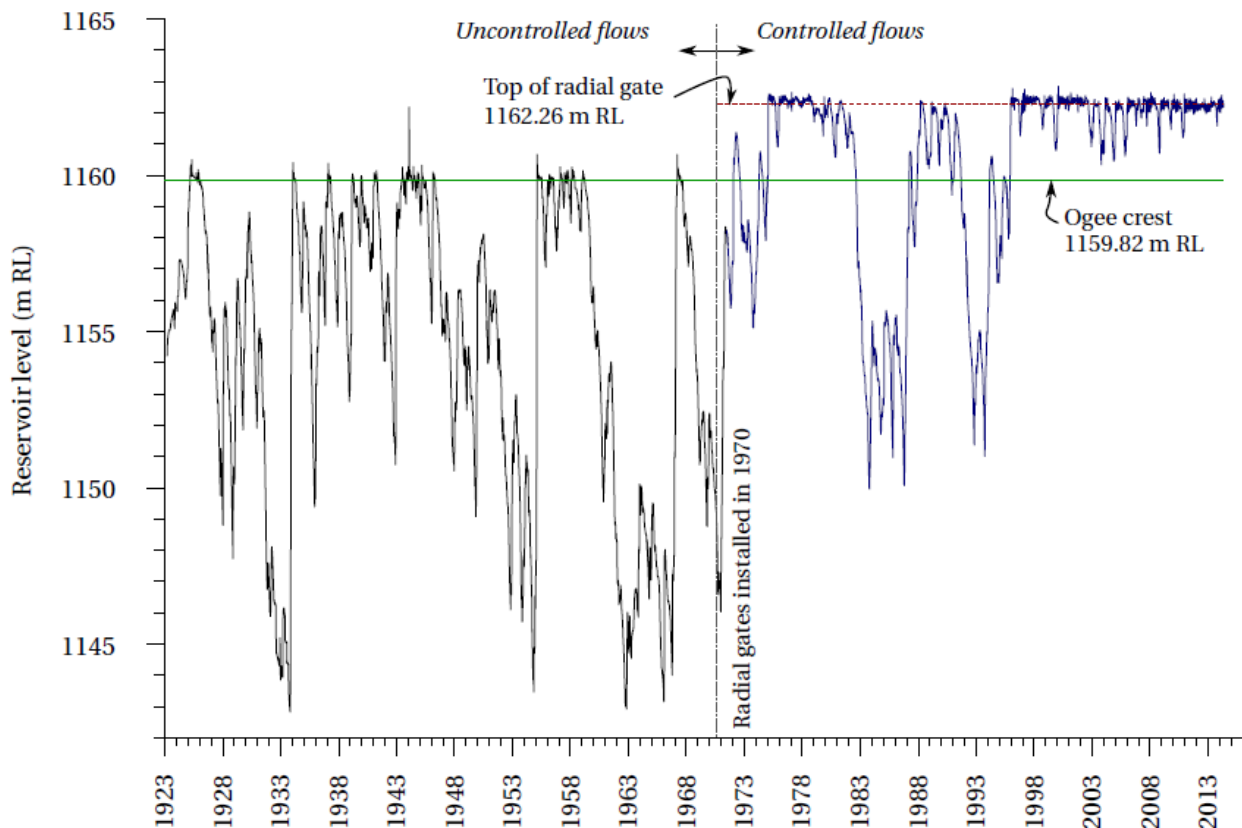


Figure 5 – Example of presentation of historical reservoir levels

### 3A. Hydraulics

It is necessary to characterise the hydraulic loading that the spillway is subject to, under historical or design flood conditions. Ultimately, it is the differential in hydraulic pressures between opposing faces of a rock unit that is responsible for scour. Integration of these pressures around the perimeter of a rock unit will resolve forces termed hydraulic 'drag' and 'lift', where drag is the force resolved parallel to the flow direction and lift is perpendicular. Calculation of these forces (in Step 5B.) requires knowledge of the flow velocity field, and for this reason it is necessary to assess flow velocity over the spillway domain. The flow discharge is usually known *a priori*, as a historical record or a design condition. The relationship between discharge, flow area and velocity depends upon the geometry of the spillway. In hydraulics, methods for analytical estimation of velocity and flow area can be grouped into three conditions: uniform flows; gradually varied (GV) and rapidly varied (RV) flows (Figure 6). Note that this analysis solves conditions for a uniform width of water and assumes depth-averaged conditions – that is, it is 1 dimensional.

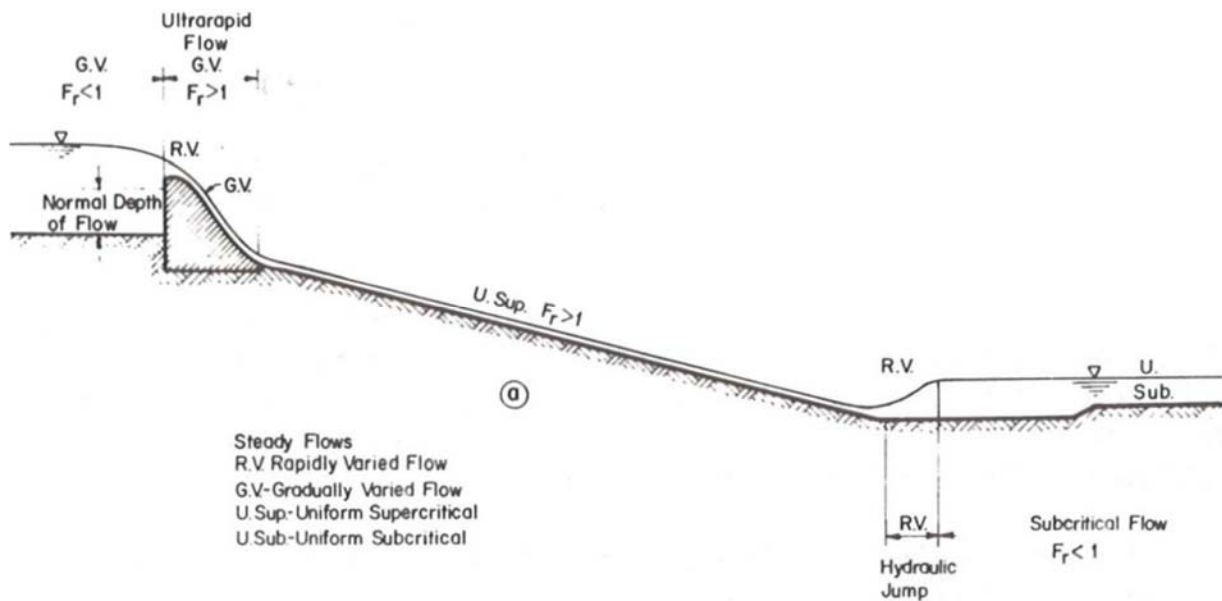


Figure 6 – Examples of gradually and rapidly varied flow (adapted from Simon and Senturk, 1976)

For uniform and GV flows, the flow velocity and depth is controlled dominantly by friction forces – a relationship that is solved through ‘hydraulic roughness equations’, such as “Manning’s” (Equation 1) or “Darcy-Weisbach” (Equation 2) equations.

$$\bar{u} = \frac{R_H^{2/3}}{n} \sqrt{S_e} \quad (1)$$

$$\bar{u} = \sqrt{8g \frac{R_H}{f} S_e} \quad (2)$$

$R_H$  is hydraulic radius (m) (flow cross-sectional area divided by the wetted perimeter);  $S_e$  is the slope of the total energy line ( $=\Delta E/L$ , where  $\Delta E$  is the dissipation of energy head (m) over the distance  $L$  (m));  $n$  is the Manning roughness parameter ( $s \cdot m^{-1/3}$ );  $f$  is the Darcy roughness parameter (dimensionless),  $g$  is acceleration due to gravity ( $m \cdot s^{-2}$ ).

The roughness parameters ( $n$  for Manning’s and  $f$  for Darcy-Weisbach) describe how quickly energy is dissipated due to friction against the bed but also due to turbulence – importantly, they are not a function of geometry and surface roughness alone, but also are a function of the flow itself. Manning’s  $n$  values are typically estimated directly from published guidance in hydraulics texts. However, such guidance is typically given for cases of relatively quiescent river flows. There is a paucity of published guidance for high-energy spillway flows. This is considered by the present writers to be an area requiring further research. Darcy  $f$  values can be estimated from absolute roughness ( $k_s$ ) values via the Colebrook-White equation – a more arduous analysis. Appropriate  $k_s$  values for unlined rock chutes also requires further research.

Uniform flows are an equilibrium condition where the energy slope  $S_e$  is parallel to the bed slope  $S_o$ , making the analysis somewhat simpler. However, uniform flow conditions seldom occur over the short and changing geometry typical to spillways. GV flow analysis is more

arduous as it requires integration of the energy balance over the channel alignment (i.e. applying the Bernoulli equation (Equation 3)).

$$z_1 + \frac{P_1}{\rho g} + \frac{\bar{u}_1^2}{2g} = z_2 + \frac{P_2}{\rho g} + \frac{\bar{u}_2^2}{2g} + \Delta E_{1-2} \quad (3)$$

$z$  is the elevation (m) of the bed above a datum;  $P$  is the pressure above the bed (Pa) and  $\Delta E$  is the dissipation of energy head (m). Subscripts indicate any two locations (1) and (2) on the channel bed.

Spillways are typically relatively short and the flows are rapid. Hence, a steady flow condition is usually a suitable assumption (that is, analysis can assume a constant discharge). Procedures for analytical estimation of GV profiles of flow depth, width and velocity using roughness equations (1) or (2) and an energy balance (3) under steady discharge are presented in many hydraulic texts. Alternatively, these solutions have also been coded into common hydrodynamic models, such as HEC-RAS.

For RV flows, energy losses are dominated by turbulent effects, and the depth profile cannot be resolved from a hydraulic roughness equation. Classical analytical solutions based on momentum considerations exist for some idealized RV flow conditions, such as for hydraulic jumps or drop structures (eg Figure 7). For example, a classical solution presented in Henderson (1966) has the solutions as shown in Equations (4 to 12)<sup>2</sup>.

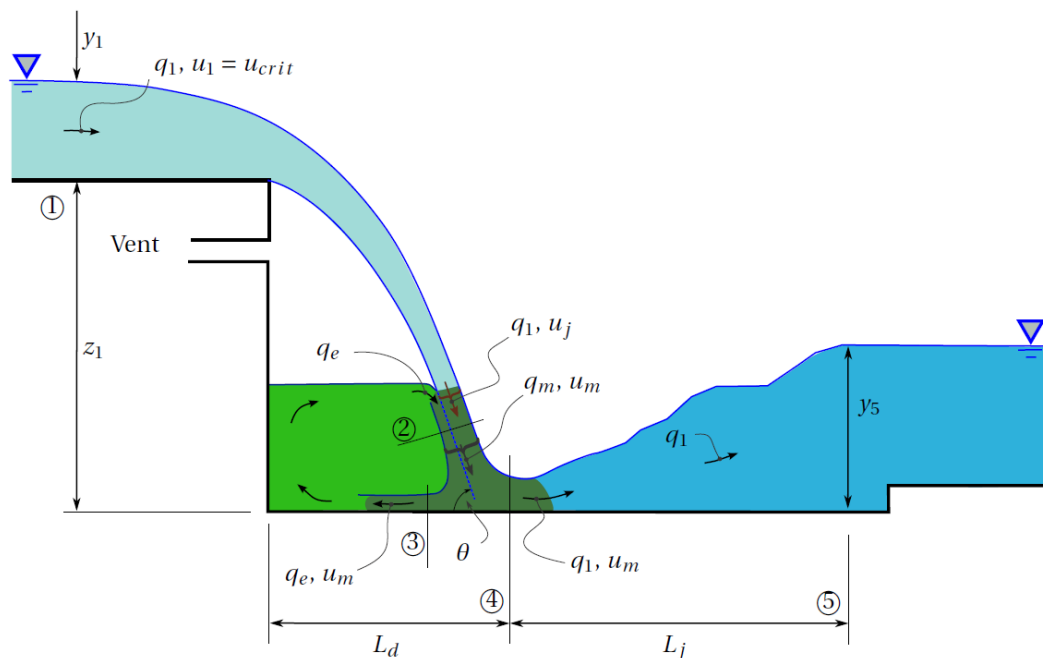


Figure 7 – Flow through a drop structure

<sup>2</sup> Derivation of these formulae are found in Appendix A of Pells (2016a).



$$y_1 = \left[ \frac{q^2}{g} \right]^{1/3} \text{ (note } y_{edge} \cong 0.715y_1 \text{ (Chow, 1959))} \quad (4)$$

$$u_j = \sqrt{2g \left( \frac{3}{2}y_1 + z_1 \right)} \quad (5)$$

$$u_m = \frac{u_j}{2} (1 + \cos \theta) \quad (6)$$

$$\cos \theta = \frac{3u_1}{2u_j} \quad (7)$$

$$y_4 = \frac{2y_1}{\frac{3}{2} + \sqrt{3 - \frac{2z_1}{y_1}}} \quad (8)$$

$$y_5 = \frac{y_4}{2} \left[ \sqrt{1 - 8F_4^2} - 1 \right] \quad (9)$$

$F_n$  is the Froude number at location  $n$  (eg  $F_1 = \bar{u}_1 / \sqrt{gy_1}$ ).

Flow velocity is used in methods that represent the kinematics of hydraulic loading, as described in Step 5B below. A method for assessment of rock-mass erosion by comparison to case studies may also be utilized (see Step 5A below), where an index is used to approximate the hydraulic loading of a flow, without representation of location-specific pressures. Various publications (eg Bagnold, 1966) have demonstrated that the rate of hydro-mechanical energy dissipation is a useful proxy for characterizing the hydraulic loading (or erosive potential) of flow. The dissipation of stream power per unit area ("unit stream power dissipation", notated herein as  $\Pi_{UD}$ ) is defined as:

$$\Pi_{UD} = \rho g \frac{Q}{B} S_e \quad (10)$$

$\rho$  is density of water ( $\sim 1000 \text{ kg.m}^{-3}$ ); and  $B$  is the width of flow (m).

$\Pi_{UD}$  can be readily assessed following the analyses of flow area and velocity. For GV flows, estimation of  $\Pi_{UD}$  is relatively straight forward, utilizing the values of  $S_e$  arising from roughness equations. For RV flows, the energy loss between selected locations can be made, for some idealised geometries, using momentum equations. For example, the energy loss between locations (1) and (4) on Figure 7 can be estimated by Equation (11) and the energy loss over a hydraulic jump (between locations (4) and (5)) can be given by Equation (12)

$$\Delta E_{1-4} = z_1 + y_1 \left[ \frac{3}{2} - \frac{2}{\alpha \sqrt{2 + \frac{3}{2}}} - \frac{\left( \alpha \sqrt{2 + \frac{3}{2}} \right)^2}{8} \right] \quad (11)$$

$$\text{where } \alpha = \sqrt{\left( \frac{3}{2} + \frac{z_1}{y_1} \right)}$$

$$\Delta E_{4-5} = y_1 + \frac{q^2}{2gy_1^2} - \frac{y_1}{2} \left( \sqrt{1 + 8F_1^2} - 1 \right) - \frac{2q^2}{g \left( y_1 \sqrt{1 + 8F_1^2} - 1 \right)^2} \quad (12)$$

Projectile theory can provide an estimation of the length  $L_d = \sqrt{2z_1y_1}$  and experimentation (eg Peterka) has shown that  $L_j \sim 6y_2$ . On this basis, the energy slope (and hence  $\Pi_{UD}$ ) can be estimated, with the solution shown in Figure 8.

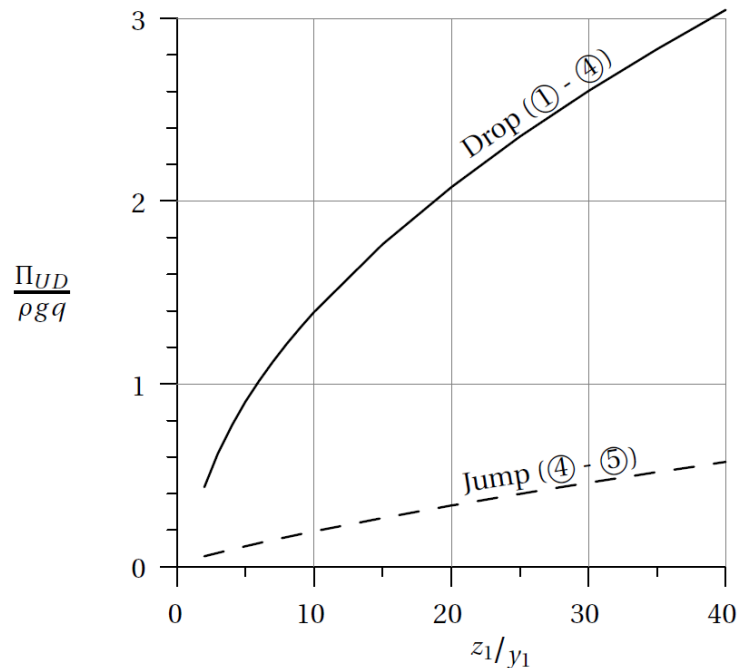


**Figure 8 – Energy slope for two rapidly varied flow cases**

The following comments are offered on estimation of  $\Pi_{UD}$

1. The estimation of the length  $L$  is the primary source of uncertainty in estimation of  $\Pi_{UD}$
2. For GV flows, estimation of  $\Pi_{UD}$  is relatively straight forward. However, changes in channel shape and bed roughness will result in peaks in  $\Pi_{UD}$  values, due to a local increase in energy gradient. These changes in should be judiciously represented.
3. Figure 8 presents the solution to the energy gradient over the classical drop structure geometry that is depicted in Figure 7, but is made under the assumption that energy is dissipated linearly over the distance  $L$ . This may not be an accurate representation of reality. The estimation of the length  $L$  for RV flow conditions is a subject requiring further research.
4. The analysis of drop structures is particular to the geometry shown in Figure 7, and is not applicable to various other tailwater conditions (e.g. Figure 9). While it is a useful solution in some cases, the particular geometry of Figure 7 is often not a suitable representation of real world spillway case studies.
5. Contrary to some practices, for plunging conditions, the dissipation length  $L$  should not be taken as the thickness of the jet, as the energy is dissipated over a much larger area, and much energy can remain after impact. In the experience of the present writers, when the 1-dimensional hydraulic conditions are analytically interpreted for spillways, the slope of the energy line rarely exceeds 3, and, except under extreme design events, the unit stream power dissipation ( $\Pi_{UD}$ ) rarely exceeds  $1000 \text{ kW.m}^{-2}$ .

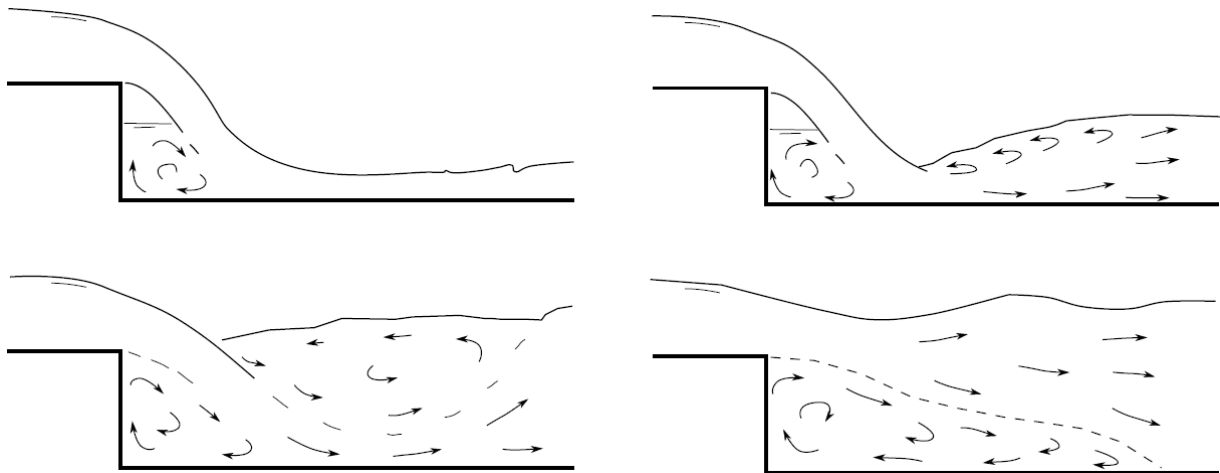


**Figure 9 – Flow conditions over a drop structure under various tailwater levels**

In summary, the above analytical methods can be used to calculate flow depths and velocity across the spillway. For GV conditions, this assessment can be made rapidly using 1D numerical hydrodynamic modelling packages (e.g. HEC-RAS or similar) which numerically resolve Equations (1) to (4). Due to the short length of the spillway domain (typically a few hundred metres) and the high velocity of water, hydraulic analyses can assume steady conditions (i.e. a constant discharge). The 1D assumption (depth and width averaged, and that the flow direction is known) is often appropriate because spillway channels are usually clearly defined. However, numerical hydrodynamic models typically will not resolve RV flow conditions suitably – the total energy at locations upstream and downstream of the RV flow section will be known (ie,  $\Delta h_{1-2}$  will be known, where (1) and (2) represent locations at either end of the RV flow section) but the rate of energy loss within the RV flow section will not be represented. For RV flow sections, outputs from 1D models should be refined with reference to analytical solutions, where suitable. In cases where no suitable analytical solution is applicable, refined estimates may require physical scale modelling, prototype measurements or detailed turbulent numerical (i.e. CFD) modelling. It should be noted that CFD simulations are not depth and width averaged, and will result in a greater spatial variation in  $\Pi_{UD}$  estimates, including regions of greater  $\Pi_{UD}$  than the averaged values estimated from analytical techniques presented above. It should be noted that the comparative assessment techniques presented in Section 5A below were developed using 1D assumptions.

It is recommended that analyses are used to plot continuous profiles of depth, velocity and energy slope across the spillway domain (e.g. Figure 2). This clearly presents the findings and also ensures that calculations maintain conservation of energy across the spillway domain. An example of presentation of spillway hydraulics based on 1D hydrodynamic models is presented in Figure 10.

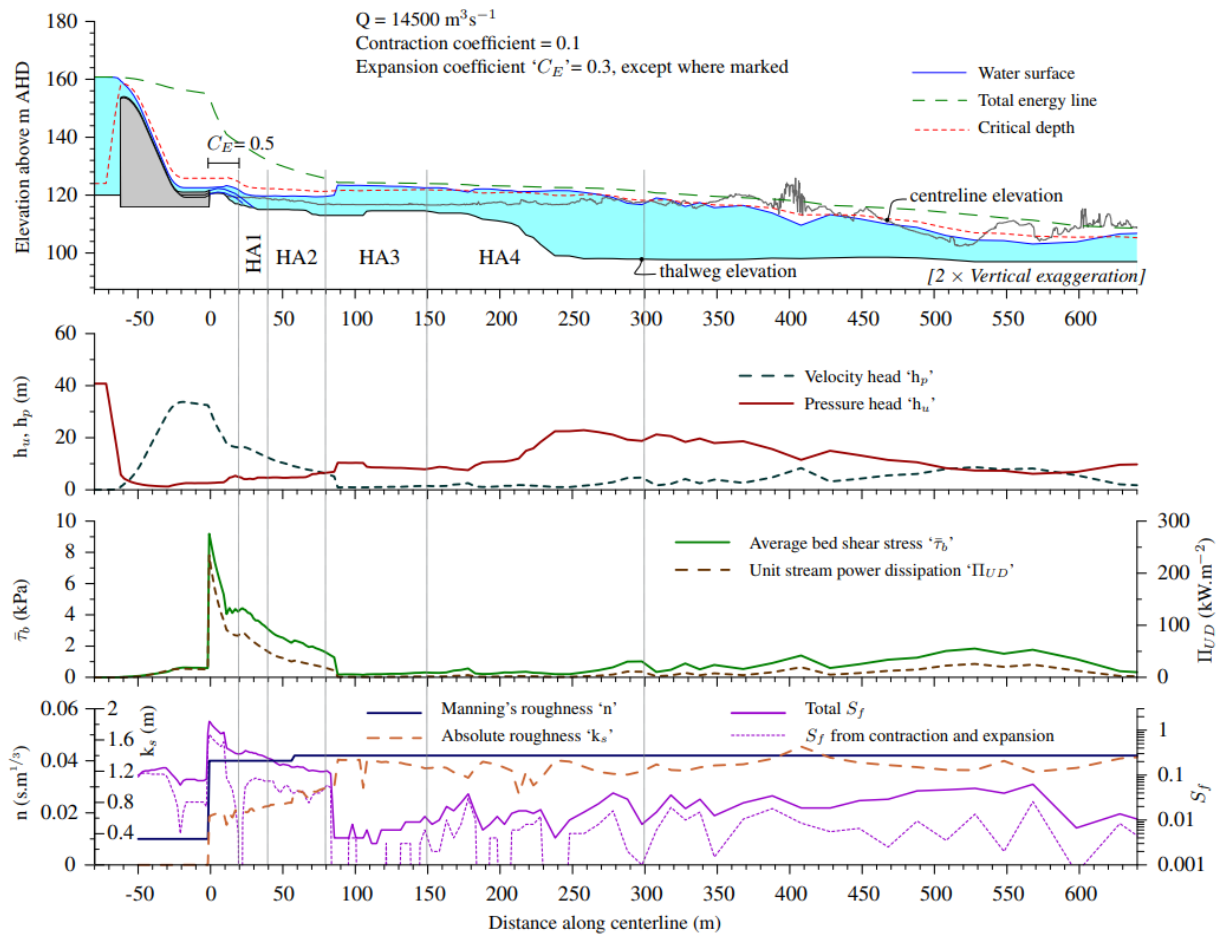


Figure 10 – Examples of presentation of hydraulic analyses

### 3B. Engineering geology

Appraisal of the geology of the unlined spillway should seek to demarcate regions of rock masses with common structural properties. This process of classification assists with creating an overall understanding of the rock mass conditions and in identifying (following the steps below) regions of higher risk. It also can assist with simplifying the analysis.

The broad discipline of geology has various ways of demarcating geological types. Of primary interest here are the structural or engineering characteristics, as evidenced by the nature of defects (ie defect type, orientation, frequency and persistence), the interaction between defect sets and the characteristics of the rock substance – its composition and strength. In some sites, different regions may be clearly apparent, but others may require detailed consideration of rock mass mapping and testing. For example, a large structural feature, such as an intrusive dyke, is clearly distinguishable from the parent rock mass. In other cases, careful consideration of fracture frequency and orientation may guide a decision to consider demarcation of regions.

Two examples of interpretation of geological domains are provided. At Mokolo Dam, in the Limpopo province of South Africa, the unlined spillway has been excavated through slightly metamorphosed horizontally-bedded sandstones, which dominate the landscape ("Domain 1"). Various thrust faults dissect the regional landscape which, due to their influence on regional topography, can be seen from aerial photographs (Figure 11). A reverse-thrust fault crosses the spillway, and its formation has locally altered the rock mass, which is pertinent to the rock-mass erodibility. As shown in Figure 12, the action of the fault has folded the bedding creating a region with defect orientations that are more vulnerable to erosion ("Domain 2"). At the fault interface, a shear zone and thin layer of clay 'gouge' also exists, creating a weak vertical plane/discontinuity in the rock mass ("Domain 3"). Three interpreted geological domains for Mokolo dam spillway are thus as shown in Figure 13 (referred to as 'structural regions' in the annotations this instance).

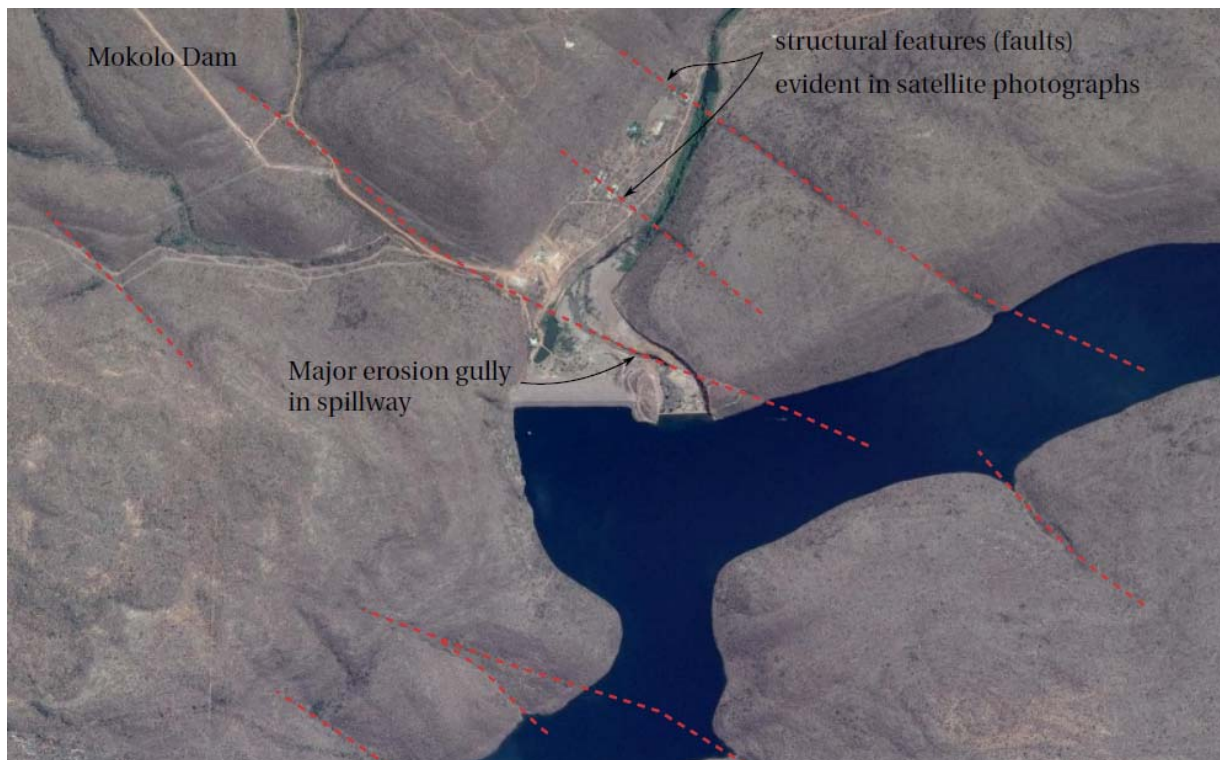


Figure 11 – Thrust faults near Mokolo Dam



Figure 12 – Down-dragged beds adjacent to the thrust fault that passes through the spillway at Mokolo Dam

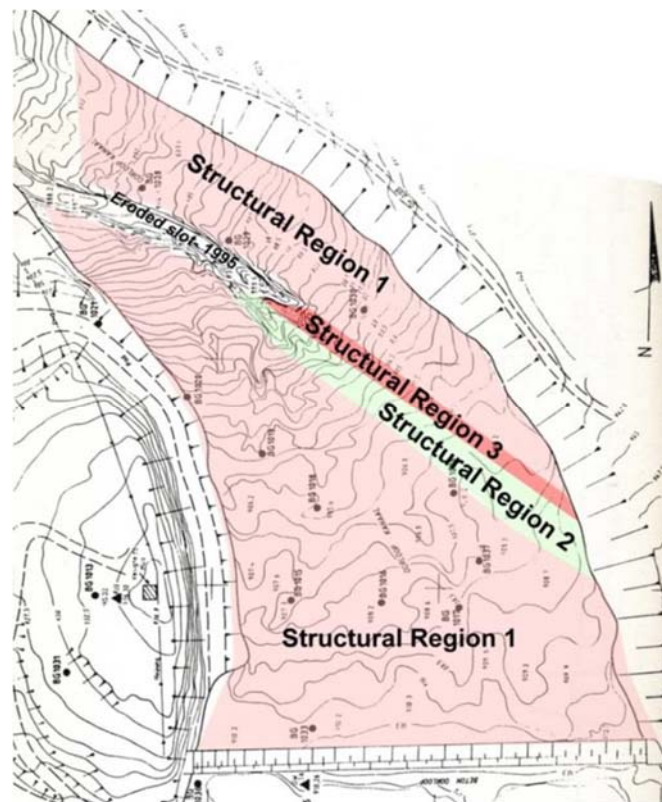


Figure 13 – Example of interpreted geological domains (or 'structural regions') for the case of Mokolo Dam

Burdekin Falls Dam, in Queensland, Australia comprises a mass concrete ogee structure (Figure 14) which discharges on to the original river bed. The bed is formed on a regional deposit of lithic ignimbrite. Visual inspection and various investigation cores show very persistent sub-horizontal defects dominate this formation. At depth, there is a relative absence of sub-vertical defects, meaning that the geology comprises massive continuous horizontal layers of high strength rock underlying the entire spillway domain. However, in places the surficial material displays increased frequency of sub-vertical fractures, perhaps from weathering and the effects of high-horizontal stresses. This surficial material is therefore distinguished from the underlying material as a different geological domain. A photograph showing these two interpreted domains is shown in Figure 15.



Figure 14 – Overview of Burdekin Falls Dam

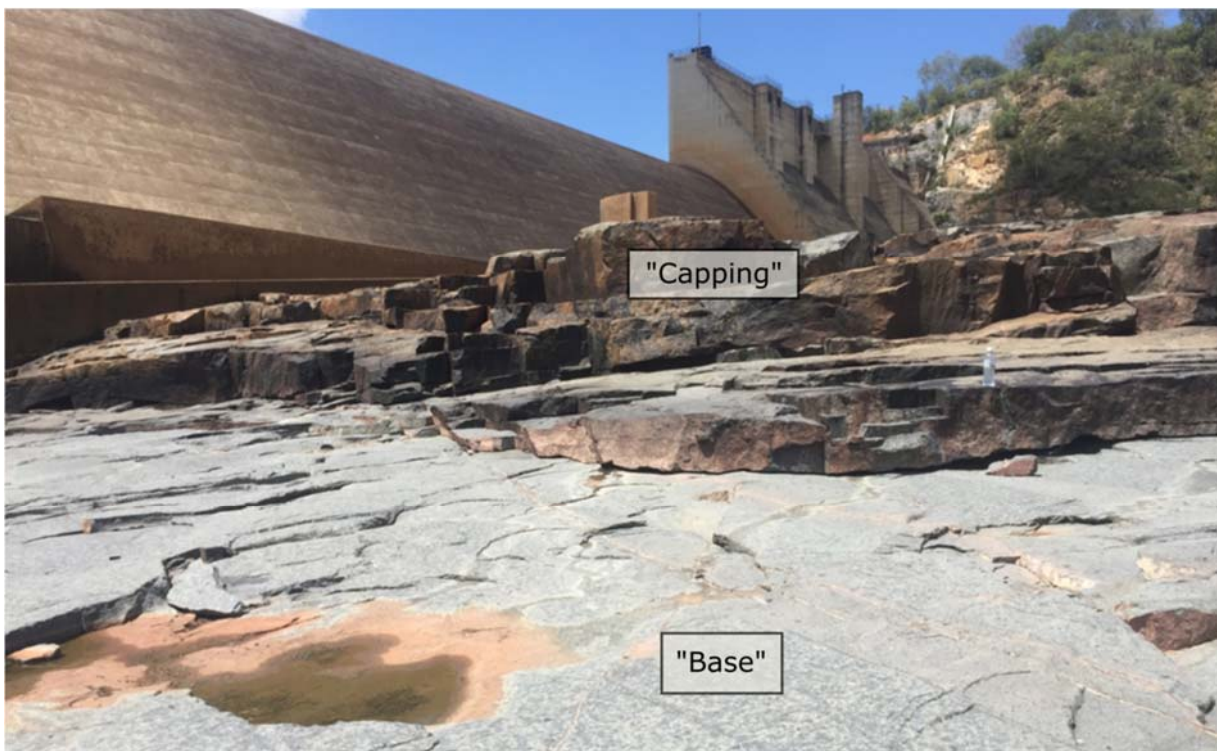


Figure 15 – Example of interpreted geological domains (Domain 1: "Capping", Domain 2: "Base") at Burdekin Falls Dam

Geological field investigations need to collect sufficient information to support the type of erosion assessment undertaken (ie. 5A, 5B and / or 5C) as described below. This would typically include (for each of the geological domains identified):

- development of defect stereoplots
- Identification of characteristic defect sets
- Measurements and/or interpretation of defect strength, frequency or spacing, persistence, roughness, aperture and infilling
- Characterization of typical rock unit shapes and orientations (as defined by defect set interaction).
- Documentation of any structural features that may be present, albeit of insufficient scale to be warranted as a separate 'domain'.
- Measurement or estimation of rock substance strength (eg UCS)

It is recommended that conceptual geological type-sections are prepared (eg Figure 16) to clearly present the interpreted geological conditions. These type-sections are required to support the analytical erosion analyses discussed in Section 5B.

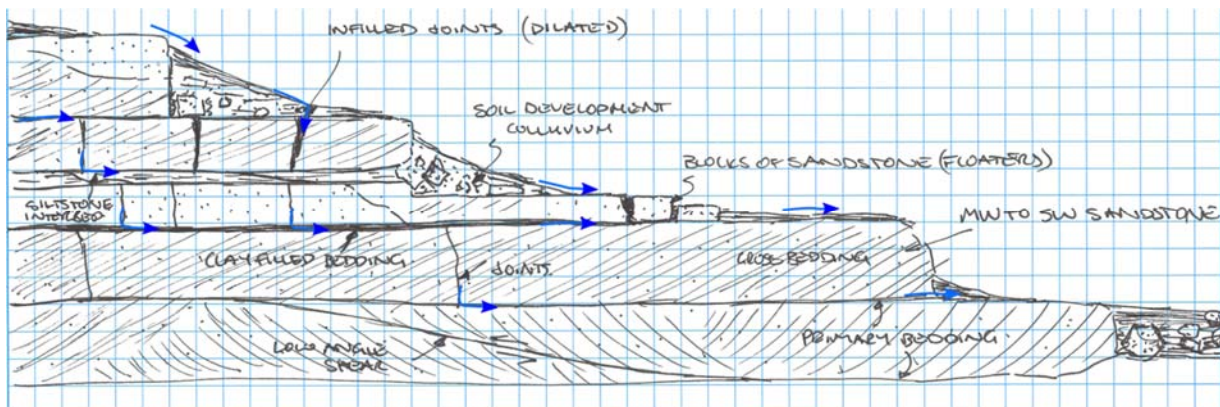


Figure 16 – Example of a geological type-section (courtesy T. Nash, PSM) Note: grid is a 1m scale

Spillways with a higher risk profile may warrant more critical analysis and therefore require more detailed geological models to be developed. For such spillways, particularly those with complex geology, 3D geological models can be developed. For existing spillways 3D numerical geological models can be prepared using specialist interpretation of photogrammetric data, and include 3D mapping of individual defects (eg Figure 17). For spillways for proposed dams, 3D geological models can be developed from geotechnical investigative data using Discrete Fracture Network (DFN) modelling techniques (eg Figure 18). It is important to remember that the DFN technique must be capable of replicating the actual interaction between defects sets (i.e. the rock mass fabric) as it directly impacts the shape of potentially erodible blocks. The application of 3D geological models in scour analysis is discussed in Section 5C below.



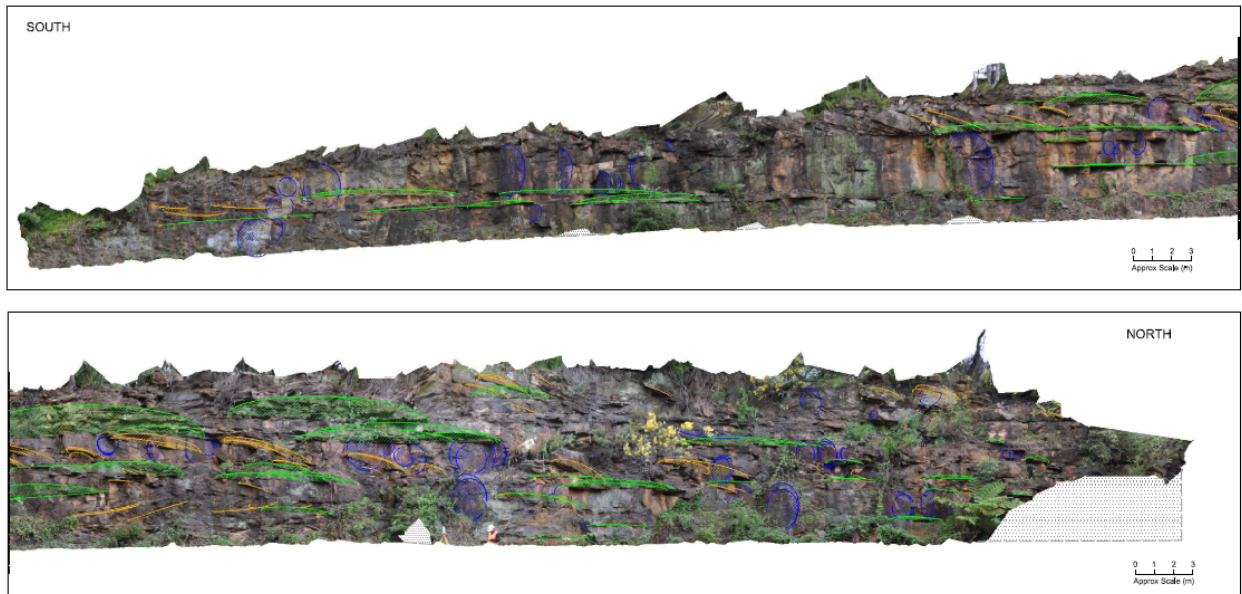


Figure 17 – Example of a development of a 3D geotechnical model from photogrammetric data (courtesy R.Brehaut, PSM)

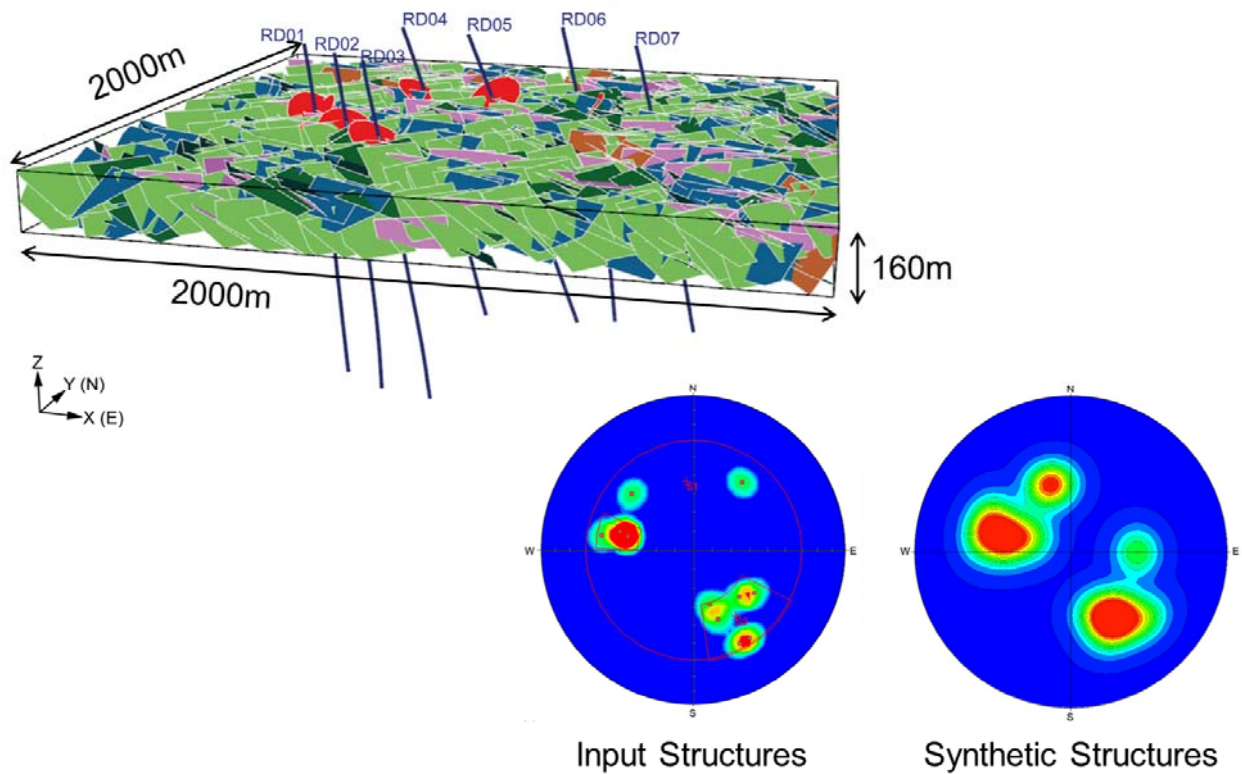


Figure 18 – Example of a development of a 3D geotechnical model from discrete fracture analysis of borehole data (courtesy Dr F. Weir, PSM)

#### 4. Scour domains

Scour domains are regions of common geology and hydraulic loading. These are determined as the intersection of hydraulic domains and geological domains. For example, a long section through the concrete gravity ogee spillway at Burdekin Falls Dam in Figure 2 (bottom) shows five designated hydraulic regions (A to E respectively). The two interpreted geological domains for this spillway are shown in Figure 15. Intersection of these interpreted hydraulic and geological domains results in definition of 8 scour domains at this spillway, as illustrated in the matrix in Table 1.

**Table 1 – Example of scour domains at Burdekin Falls Dam, based on the interpreted hydraulic domains shown in Figure 2 (bottom) and geological domains shown in Figure 15**

			Geological domains	
			1	2
			“Capping”	“Base”
Hydraulic domains	A	Flip bucket	-	-
	B	Backroller	B1	B2
	C	Jet impact zone	C1	C2
	D	Dissipation zone	D1	D2
	E	Tailwater zone	E1	E2

It is only necessary to define scour domains where the onset of scour would be of possible consequence to dam safety. For example, for the generic case shown in Figure 2 (top), scour domains could be defined as per Table 2 – there may be no requirement to assess scour in the original river bed, for instance.

**Table 2 – Example of determination of scour domains based on the generic case in Figure 2 (top)**

			Geological domains			
			Spillway Excavation zone		Natural slope	
			1	2	3	4
			Blast affected	fresh	weathered	fresh
Hydraulic domains	A	Impact / jump zone	A1	A2	-	-
	B	Excavation uniform flow	B1	B2		
	C	End-of-excavation knickpoint	C1	C2	C3	C4
	D	Natural hillslope uniform flow	-	-	D3	D4
	E	Tailwater zone	-	-	-	-

Geological Domains 2. and 4. in Table 2 only come into play if erosion removes upper Domains 1. and 2. Significant reshaping of the spillway from scour may create new hydraulic conditions, such as plunging or channelization, which may require recognition of new domains subsequent to erosion. Pells et al (2016) noted that such a positive feedback loop between reshaping (from scour) and changed hydraulic conditions was responsible for very large scour in some instances,

such as Mokolo Dam, introduced above, and Copeton Dam in Australia. For example, erosion of the fault zone at Mokolo Dam created channelized and plunging flow conditions, which incurred greater hydraulic loading, leading to further scour and so on. The possibility of such an occurrence, particularly for lineal geological structures, should be perceived in the process of defining scour domains.

### **5A. Comparative scour assessment**

Three methodologies for assessment of rock scour are discussed in Section 5A, 5B and 5C. The first, discussed here, has been termed by the present writers as a 'comparative' method, because it assesses erosion through comparison to case studies, where the rock mass conditions are compared using a rock mass Index, and the hydraulic conditions using the unit stream power dissipation. Neither the rock-mass index nor the stream power dissipation describe the problem completely, but have been shown to be useful indicators, or proxies, of general conditions.

A rock-mass index is a system that attempts to describe the engineering characteristics of a rock mass with a single number. A numerical rating of the rock-mass is obtained from the sum or product of various numbers which are chosen (with reference to specific guides and tables) to represent the orientation, quantity and condition of joints in the rock mass and the strength of the rock substance. Two early examples of rock-mass indices are the Rock Mass Rating (RMR) system (Bieniawski, 1973) and the "rock-tunnelling quality index" (the Q-system) (Barton et al 1974). These rock-mass indices were originally developed for tunnel support design and are still widely used for that purpose today. Numerous other rock-mass indices have since been developed for other applications, most of which are extensions or modifications on RMR or Q-system. The Geological Strength Index (GSI) (Hoek et al, 1995) is a modification to the RMR system and also enjoys wide usage within the discipline of engineering geology. Rock mass indices are recognized as offering a limited representation of the rock mass, but are still considered useful for some purposes of communication and comparison (Hudson and Harrison, 2000). Various researchers have used rock mass indices as an indicator of erodibility (Kirsten and Moore, 1988; Pitsiou, 1990; Moore, 1991; Dooge, 1993; van Schalkwyk, et al 1994; Annandale 1995; Kirsten et al 2000). In most of these cases, the researchers utilized the Kirsten Index, which is a rock mass index based on the Q-system (Kirsten 1982), modified to represent excavatability of rock masses. The Kirsten index has been largely forgotten within the rock-mechanics / engineering geology fraternities.

Research undertaken in Australia between 2012 to 2016 (Pells, 2016a) examined if currently used rock-mass indices were suitable indicators of erodibility of rock masses. For this research, a dataset of 118 observed rock mass erosion instances was collected from field investigations at dam spillways in Australia, South Africa and USA. Interpretations of RMR, Q, and GSI were made of each case. Analysis of this dataset confirmed that the observed erosion correlated to each of these rock-mass indices – i.e. with better quality rock typically offering higher erosion resistance. The strength of correlation was similar for all these indices (and also for the Kirsten Index). The data were then used to develop two new rock mass indices to represent rock mass erodibility. These two systems could then be employed within a new 'comparative' method, as

described below. In each case, the extent of erosion is assessed in terms of five classes, as described in Table 3, reflecting the nature of erosion as observed at these case study sites.

**Table 3 – Erosion risk classes**

Class	Erosion descriptor	Maximum erosion depth (m)	General erosion extent (m <sup>3</sup> per 100 m <sup>2</sup> )
I	Negligible	< 0.3	<10
II	Minor	0.3 - 1	10-30
III	Moderate	1 - 2	30-100
IV	Large	2 - 7	100-350
V	Extensive	> 7	>350

### eGSI

The Geological Strength Index (GSI) (Hoek et al, 1995) was found to provide a useful indication of rock mass erodibility (Pells, 2016). Moreover, it was found that GSI values interpreted by usage of a simple lookup chart (Figure 19) were consistent to GSI obtained by the more complex calculation. This finding is consistent with Bertuzzi et al 2016 and Pells et al 2017. The GSI chart is also significantly simpler to use, and allows an estimation of GSI to be made without requiring RQD, which is a factor that was found to be particularly sensitive to operator subjectivity (Pells, et al 2017).

However, GSI does not represent the orientation of rock mass defects which was found to be an important factor in observed case studies of rock mass erosion. A better representation of rock-mass erodibility was obtained by modifying GSI with an appropriate orientation adjustment factor, which was developed through examination of various erosion case studies as well as the results of laboratory testing (Pells, 2016). The resulting erodibility GSI ('eGSI') is thus determined as:

$$eGSI = GSI + E_{doa} (>0) \quad (13)$$

Where:

- GSI is the ground strength index, estimated using the chart method (Hoek and Marino, 2000) (reproduced as Figure 19 below)
- $E_{doa}$  is a discontinuity adjustment for erodibility, estimated from Figure 20 or 21 (as appropriate)

Figure 22 shows the observed erosion from 118 case studies plotted according to their interpreted eGSI and hydraulic ( $\Pi_{UD}$ ) conditions. Interpreted contours of erosion class (as per Table 3) are also shown. An estimation of erosion vulnerability can thus be made by plotting the interpreted  $\Pi_{UD}$  and eGSI conditions for a case in question, and noting which erosion class the conditions fall within. This can be repeated for each scour domain. Note that the case studies for each data point can be found in Pells (2016a).

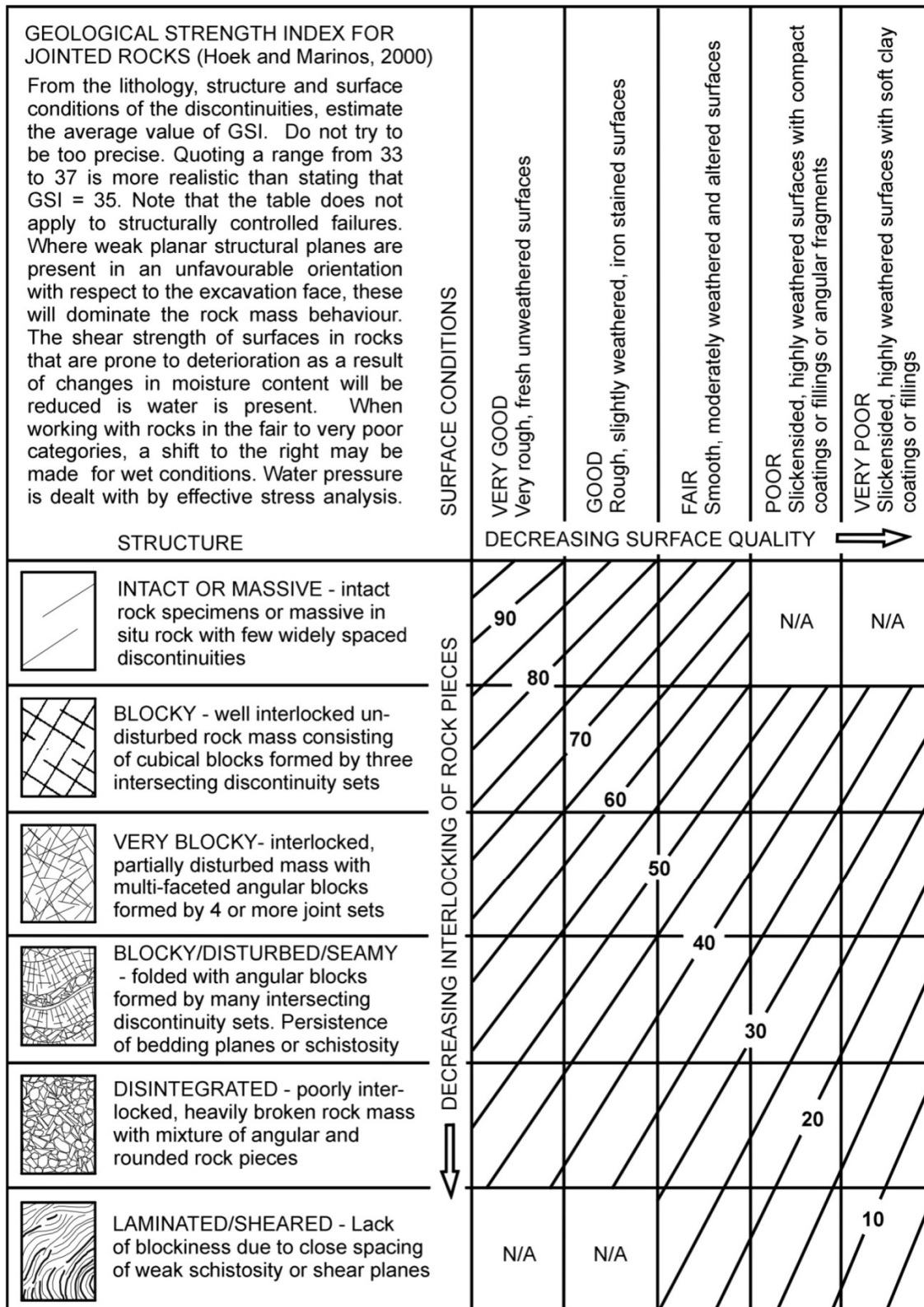


Figure 19 – Chart for characterization of GSI of blocky rock masses on the basis of interlocking and joint conditions (Hoek, 2006)

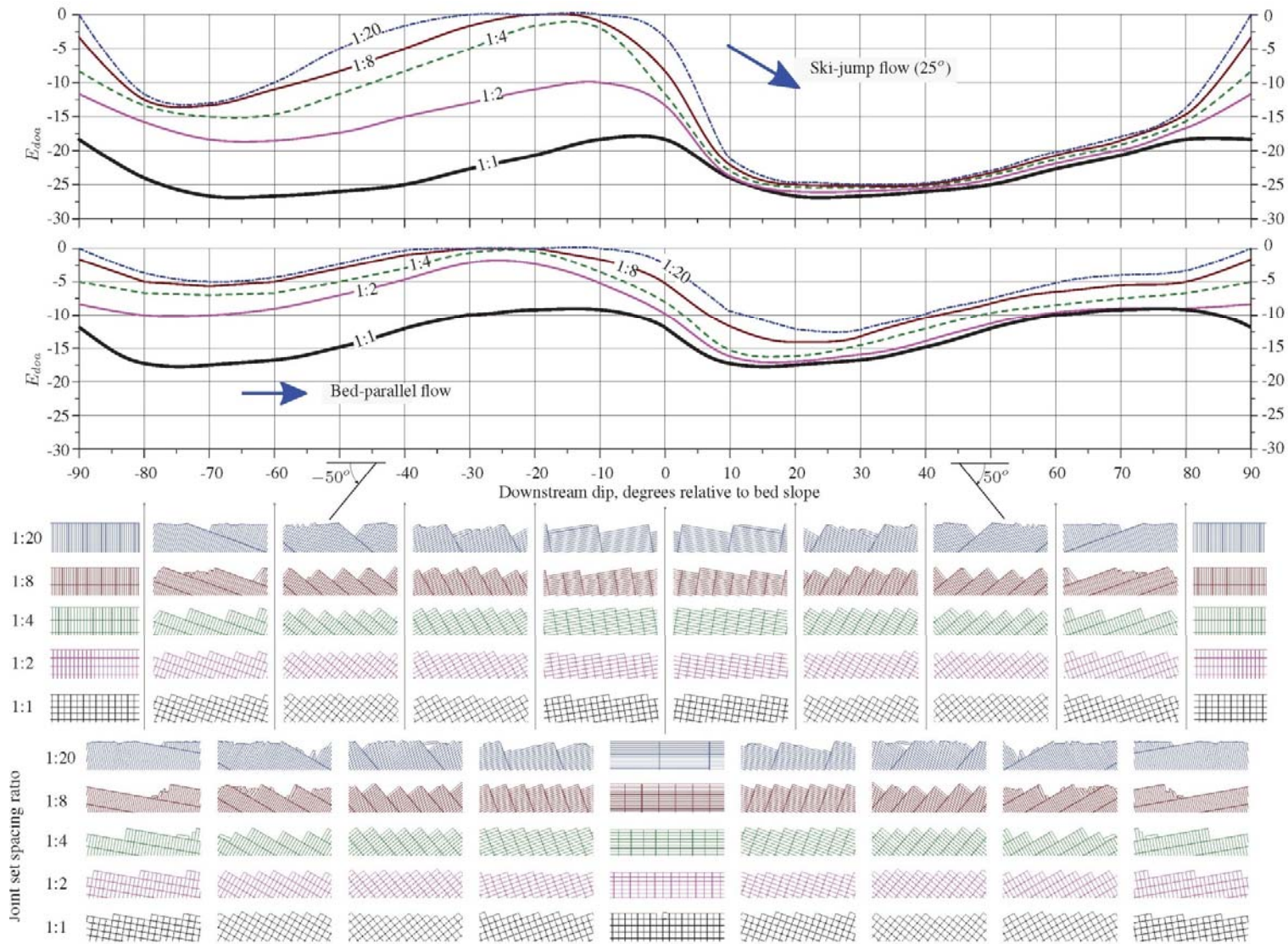


Figure 20 – Discontinuity orientation adjustment for erosion ('eDOA') for horizontal beds

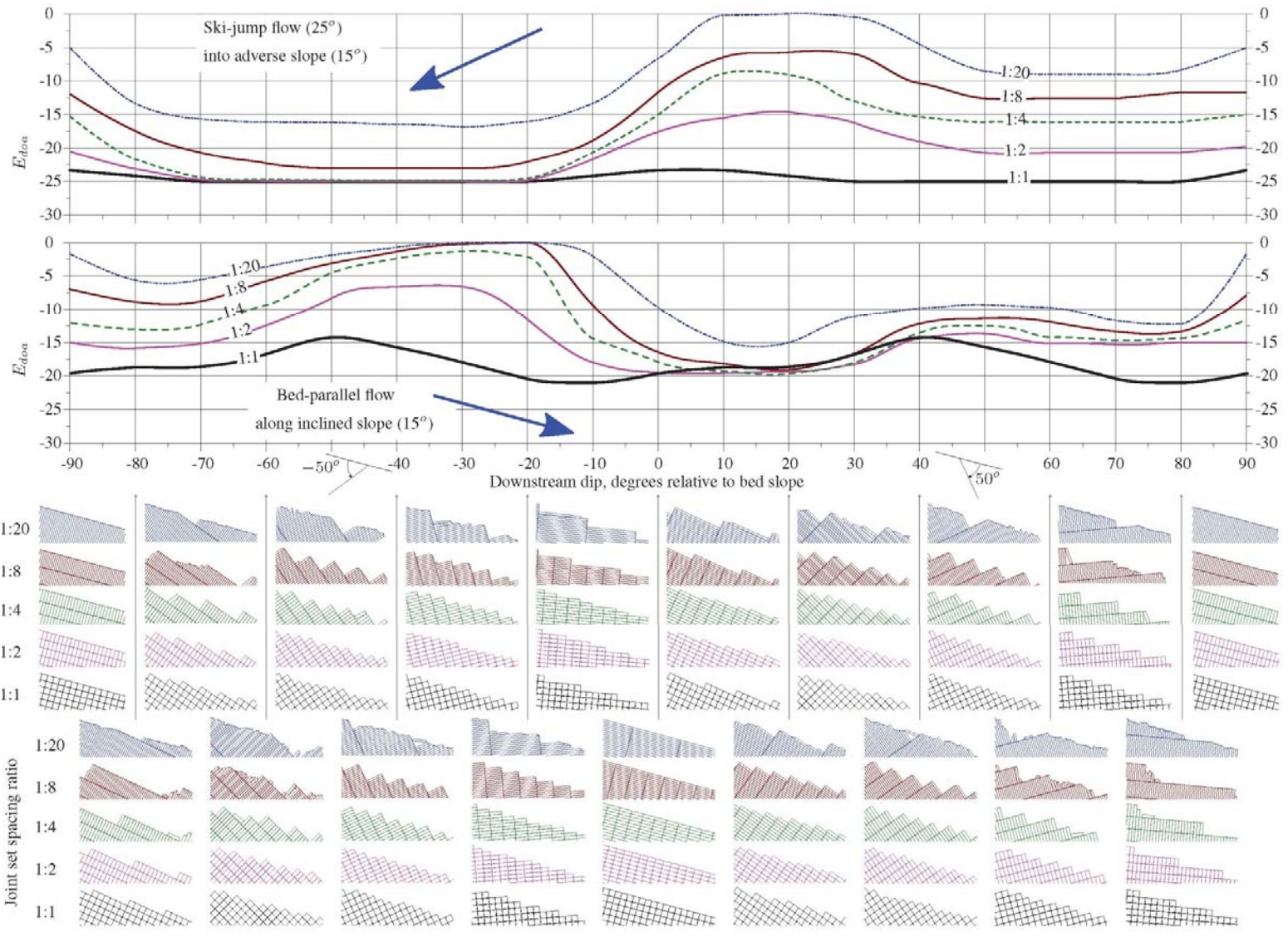


Figure 21 – Discontinuity orientation adjustment for erosion ('eDOA') for inclined beds

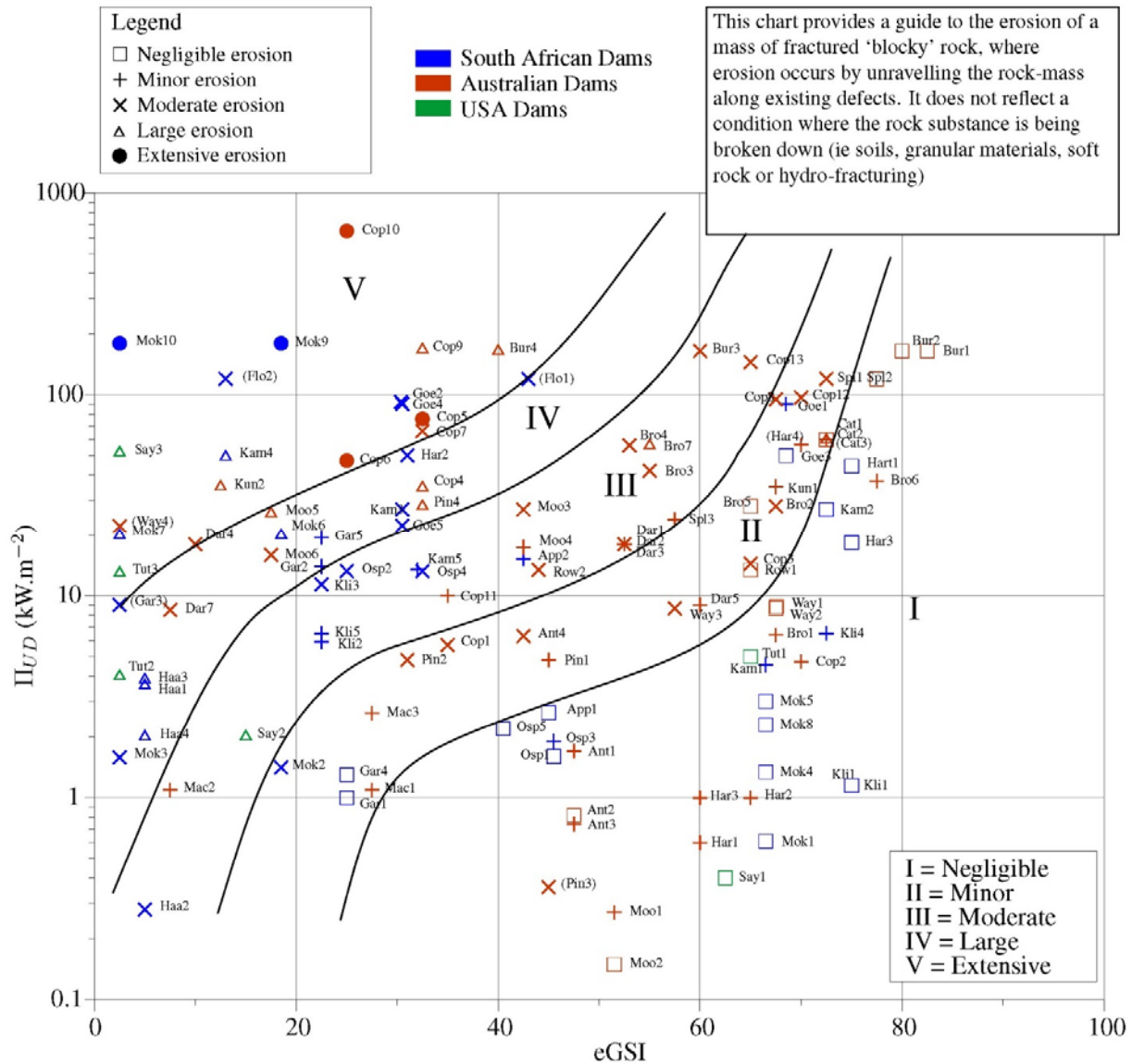
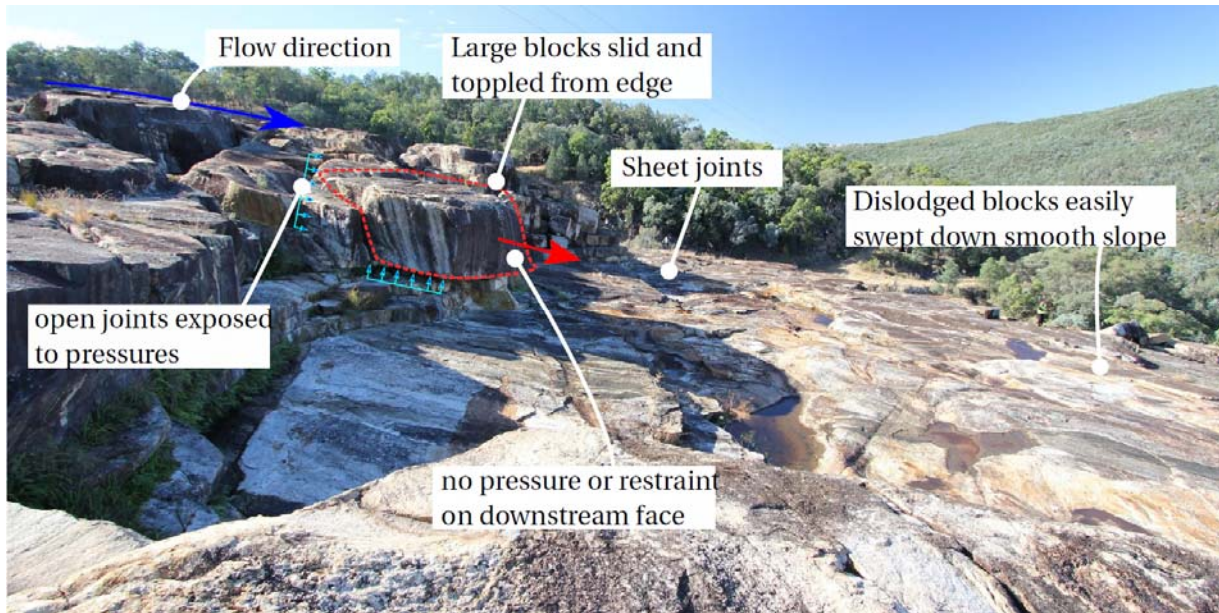


Figure 22 – Rock-mass erodibility assessment chart using eGSI

### RMEI

In review of case studies, various geometric conditions were observed to create vulnerability to erosion. The orientation of defects relative to the spillway determines the vulnerability to stagnation pressures from high velocity flow, and also the presence mechanisms of detachment or slope instability. For example, consider the photograph in Figure 23 from Copeton Dam, Australia. Rock mass indices as described above may communicate something about qualities of the rock mass, but would not describe that large blocks are poised on the edge of a slope, being vulnerable to hydraulic stagnation pressures on its upstream face, and translational sliding down the slope.





**Figure 23 – Examples of mechanisms of unravelling in an unlined spillway**

A system was developed which attempts to identify the presence of vulnerabilities in unlined spillways based on defect characteristics and spillway geometry. The resulting index, termed the Rock Mass Erodibility Index (RMEI) was developed based on the observed geological factors controlling detachment of blocks in unlined spillways in rock. The method was developed progressively using case study data with several refinements of the factors and their description. This was done initially with little account of the history of spillway flows and resulting hydraulic loads. Later in the development process these loads were introduced using  $\Pi_{UD}$  as an indicator. The structure of the system was based upon that used in Fell *et al.* (2008) for estimating the probability of internal erosion and piping in dams and found there to be useful for combining multiple qualitative factors to assess likelihoods, in this case for predicting the likelihood of detachment of blocks of rock from the spillway floor.

Table 4 presents the erosion vulnerability factors, their interpreted importance, and likelihood factors which are described for each of the vulnerability factors. Table 5 provides a suggested method for estimating the nature of the defects (erosion vulnerability factor  $F_3$ ). The erosion is quantified as erosion classes as detailed in Table 3. It should be noted that, as for eGSI, the method is not designed to be binary i.e. erosion occurs or does not occur. The observations in the case data is that erosion has occurred in all of the spillways and even within one spillway several erosion classes may apply to different erosion domains.

As described in Pells (2016a) two expressions for RMEI were trialed based on alternative mathematical operations of LF and RF. The adopted RMEI in equation (7) gives a somewhat better outcome and the expression fits better to a risk based logic and gives a wider spread of RMEI values so has been adopted.

$$RMEI = [RF_{P_1} \times LF_{P_1}] \times [RF_{P_2} \times LF_{P_2}] \times [(RF_{P_3} \times LF_{P_3}) + (RF_{P_4} \times LF_{P_4}) + (RF_{P_5} \times LF_{P_5})] \quad (7)$$

The possible range of RMEI values calculated from Equation (7) is 36 to 4500. Low RMEI indicates geological conditions are resistant to erosion whereas high RMEI indicates geological conditions are conducive to erosion.

RMEI values were assessed at erosion domains at 23 dam spillways, representing 101 data points. In Figure 24 the case study data are plotted as a function of RMEI and  $\Pi_{UD}$ , and contours were drawn with respect to the observed erosion class.

The erosion class contours in Figure 24 follow those presented in Douglas et al (2018), which were modified from what was presented in Pells (2016a). This was to allow for the following:

- (a) From sediment transport / geomorphological studies, 100 W/m<sup>2</sup> is the lowest stream power associated with initiation of sediment movement. Hence the curves have been assumed to asymptote to this value even for rock with high RMEI.
- (b) For RMEI = 0, intact rock studies by Kirsten indicated values of 10000 to 100000 kW/m<sup>2</sup> for erosion of intact materials – the contours upper range reflects this.
- (c) The quality of the data points near the erosion class boundaries.

It can be seen that the erosion class contours correlate reasonably well with the data for erosion classes I, II and III and less so for classes IV and V. The boundary for class V is least well defined as there are fewer data points.

Worked examples for comparative scour assessments using eGSI and RMEI are presented below.

**Table 4 – RMEI relative importance (RF) and likelihood factors (LF)**

Erosion vulnerability parameter	Relative importance Factor (RF)	Likelihood Factor (LF)				
		Very Unlikely	Unlikely	Likely	Highly Likely	Almost Certain
		1	2	3	4	5
F1: Kinematically viable mechanism for detachment <sup>1</sup>	3	Rock with three defects, basal defect sub-parallel to spillway floor, and no day lighting basal release surface, or; Massive rock with effectively only two defect sets and no basal release surface.	Rock with three or more defects, with: basal defect sub-parallel to spillway floor, Joint 2 protruding from surface, or; Basal defect inclined upstream or downstream at > 30 degrees relative to spillway floor.	Rock with three or more defects, with: persistent basal defect dip 10 to 30 degrees upstream relative to the spillway floor, or; Persistent basal defect dip 10 to 30 degrees downstream relative to the spillway floor.	Rock with three or more defects, with: persistent basal defect dip ≤ 10 degrees upstream relative to the spillway floor, or; Persistent basal defect dip ≤ 10 degrees downstream relative to the spillway floor.	Persistent basal defect sub-parallel to the spillway floor, day lighting upstream or downstream, or; Persistent shear and/or closely jointed rock which erodes readily forming a release surface into the shear.
F2: Nature of the potentially eroding surface	3	Smooth water or glacier worn, with no protrusions of joint 2, no opening of defects	Bedding surface with protrusions of joint 2 < 1mm, and little or no opening of defects	Relatively small protrusions and defect openings (e.g. pre-split, or ripped and bulldozed)	Irregular surface following defects, little opening of defects (e.g. blasted rock)	Irregular surface following defects, extensive defect opening (e.g. heavily blasted rock)
F3: Nature of the defects <sup>2</sup>	2	Very rough surfaces, e.g. JRC ≥ 12	Rough surfaces, e.g. JRC 8-10	Slightly rough surfaces e.g. JRC 4-8	Smooth surfaces e.g. JRC < 4	Smooth or slickensided surfaces
		No separation	Aperture < 1mm	Aperture 1-2mm	Aperture 2 to 5mm	Aperture > 5mm
		UCS > 50MPa	UCS 20MPa to 50MPa	UCS 5MPa to 20MPa	UCS 1MPa to 5MPa	UCS < 1MPa, or Soft gouge > 5mm thick
F4: Spacing of basal defect <sup>3</sup>	1	> 3m	1m to 3m	0.3m to 1m	0.1m to 0.3m	< 0.1m
F5: Block shape <sup>4</sup>	1	≤ 0.5	0.5 to 1	1 to 2	2 to 5	> 5

Notes:

1. Defects include joints, bedding surfaces, shears, and foliation partings.
2. Select class which best fits the data taking into account the kinematically viable mechanism and which defects control the displacement of the block of rock from the spillway.
3. Joint 1 is basal defect of a block or region (bedding or joint).
4. Block shape = Joint 2 spacing / Joint 1 spacing; Joint 2 is sub-vertical defect normal to the flow in the spillway.

Table 5 – Suggested method for estimating F3 'Nature of defects' (Table 4)

Separation	Joint Roughness Coefficient (JRC)				
	>12	8 to 10	4 to 8	<4	Smooth and/or slickensided
Tight, no separation	1	1	1	2	2
< 1mm	1	1	2	3	3
1 to 2mm	1	2	3	4	4
2 to 5mm	2	3	4	5	5
>5mm	3	4	5	5	5

Notes:

1. If joint is in-filled with soil, or is weathered to UCS < 1 MPa, assume in-fill and / or soil is eroded and use eroded opening as separation.
2. If joint walls have UCS 1 MPa to 5 MPa, increase relative importance factor by 1, with a maximum of 5.
3. Joint Roughness Coefficient to be estimated from Barton and Bandis (1991).

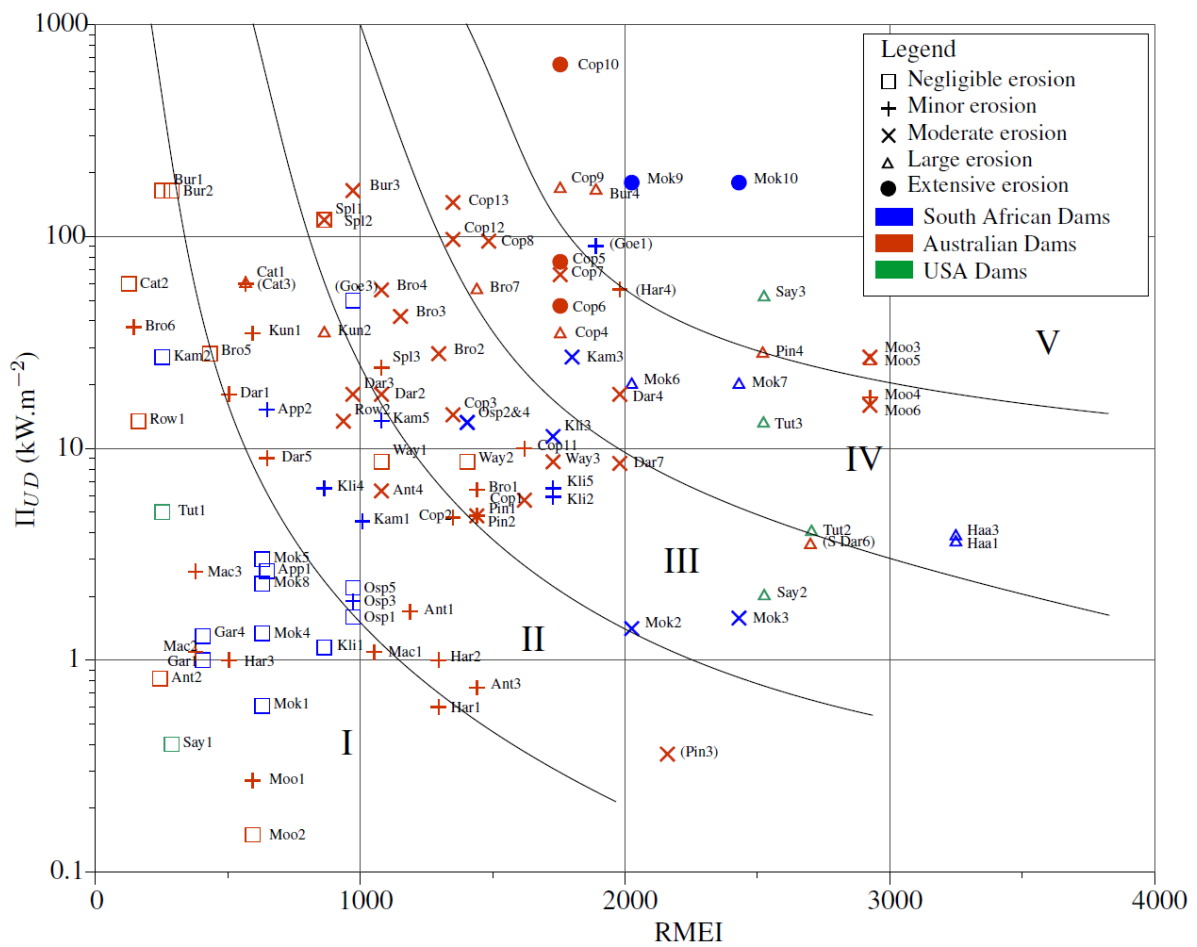


Figure 24 – Rock-mass erodibility assessment chart using RMEI

## A worked example of comparative scour analysis

The 'comparative' analysis presented below is for the scour domains shown in Table 1 above, at Burdekin Falls Dam, Australia. The assessments adopt the values of  $\Pi_{UD}$  presented in Table 6.

**Table 6 – Estimated  $\Pi_{UD}$  values for comparative assessments**

Event	Discharge $m^3.s^{-1}$	$\Pi_{UD}$ ( $kW.m^{-2}$ )		
		Impact Zone	Transition (Jump) Zone 50 to 80 d/s	80 to 200 d/s
Typical annual event	5000	100 to 200	50 to 150	5 to 25
Flood of record	18400	180 to 250	80 to 175	50 to 100
DCF 1:4500 AEP	69600	240 to 350	175 to 240	100 to 150
PMPDF 1:9900 AEP	97900	250 to 350	200 to 250	100 to 175

eGSI values were interpreted for the two geological domains. The values of GSI selected are shown in Figure 25. The values of  $E_{doa}$  selected are shown in Figure 26. The values of eGSI from substitution of these values into Equation 6 are shown in Table 7.

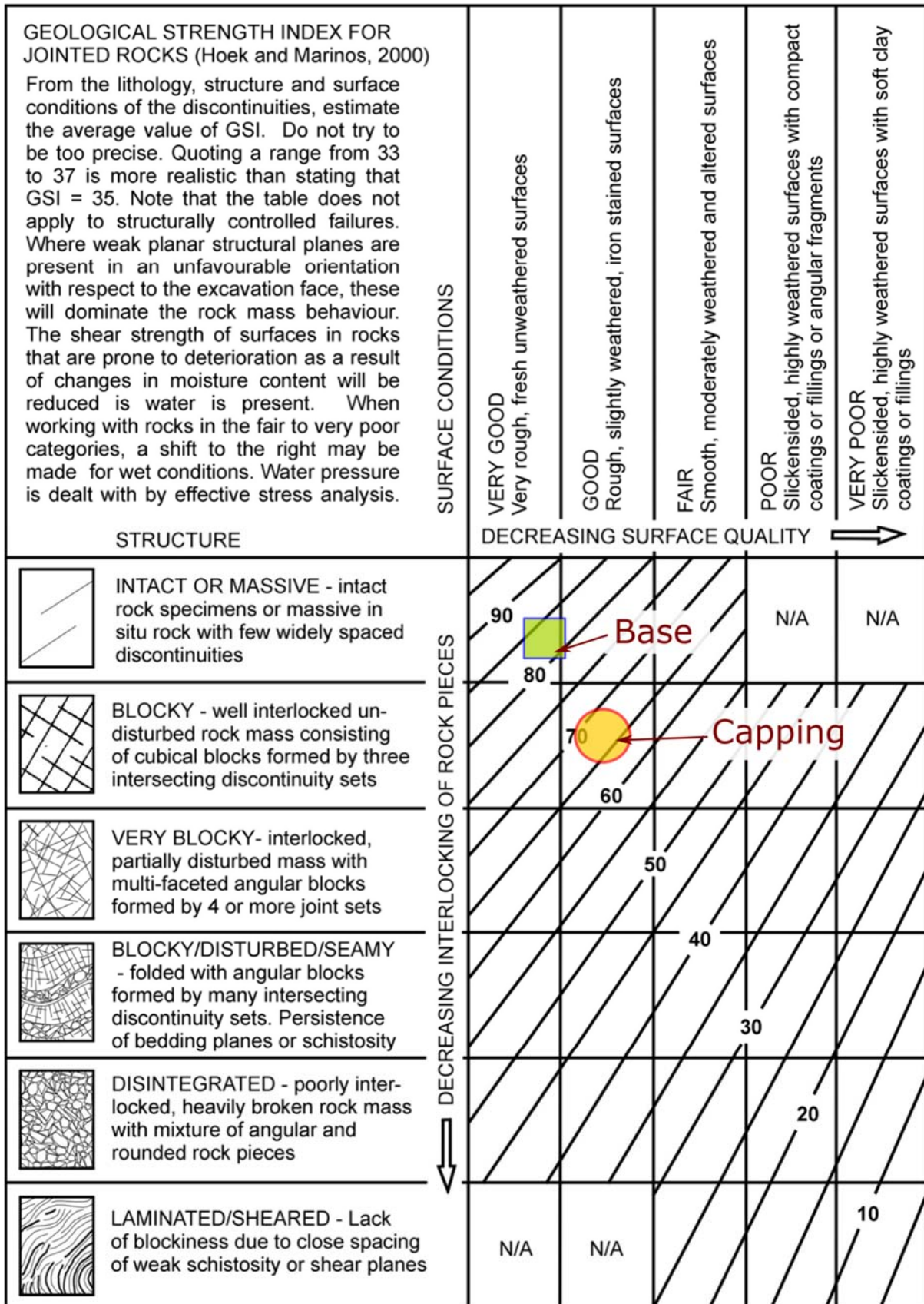
Vulnerability to scour is assessed by plotting the assessed values of eGSI and  $\Pi_{UD}$  on the eGSI chart. These charts are reproduced in Figure 27, Figure 28 and Figure 29 for the three regions of spillway shown in Table 6. The assessed erosion classes for selected flood events are summarised in Table 8.

**Table 7 – Assessed eGSI values for Burdekin Falls Dam**

	Impact Zone		Elsewhere	
	Capping	Base	Capping	Base
GSI	65-70	80+	65-70	80+
$E_{doa}$	-13	-7	-10	-5
eGSI	52-57	73+	55-60	75+

**Table 8 – Assessed eGSI erosion classes for Burdekin Falls Dam**

	Impact Zone		Transition (Jump) Zone 50 to 80 d/s		80 to 200 d/s	
	Capping	Base	Capping	Base	Capping	Base
Flood of record	IV	II	III	I/II	III	I
PMPDF 1:9900 AEP	IV	II	IV	II	III	I



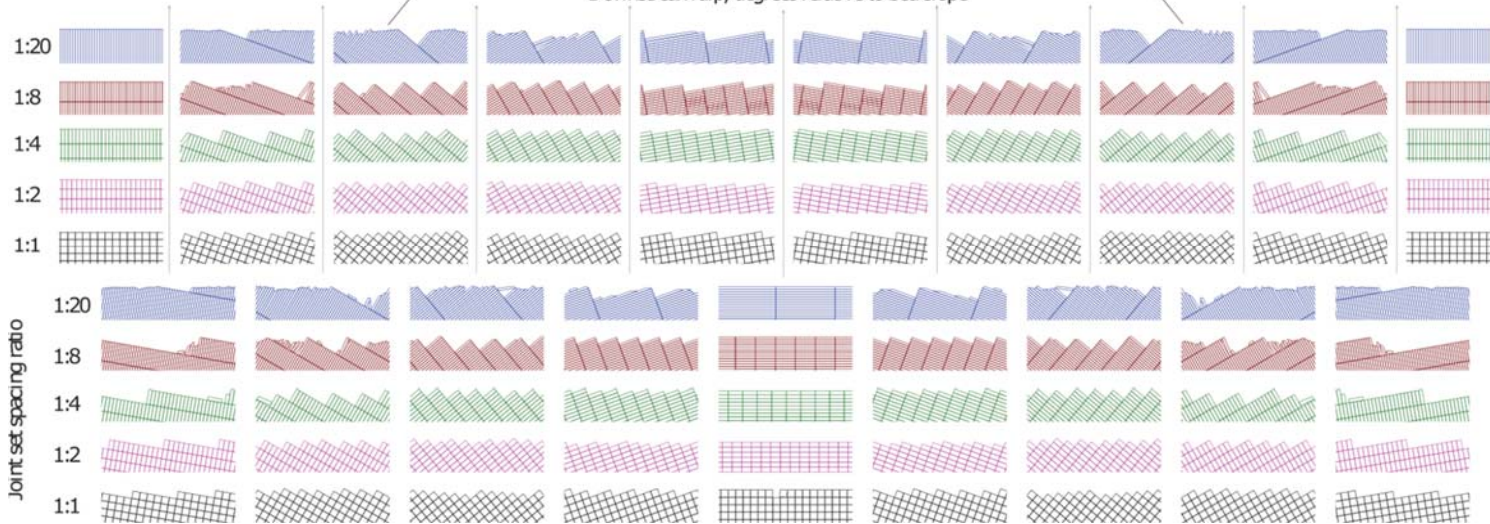
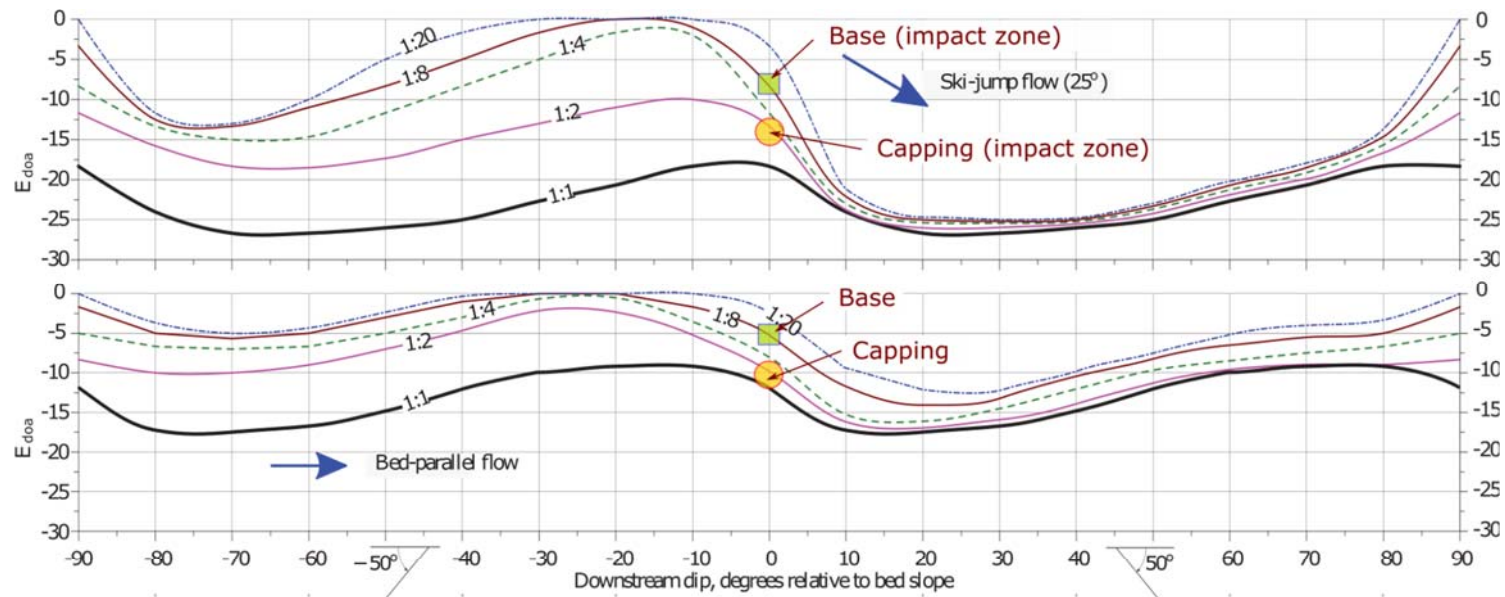


Figure 26 -  $E_{doa}$  values interpreted for Burdekin Falls Dam

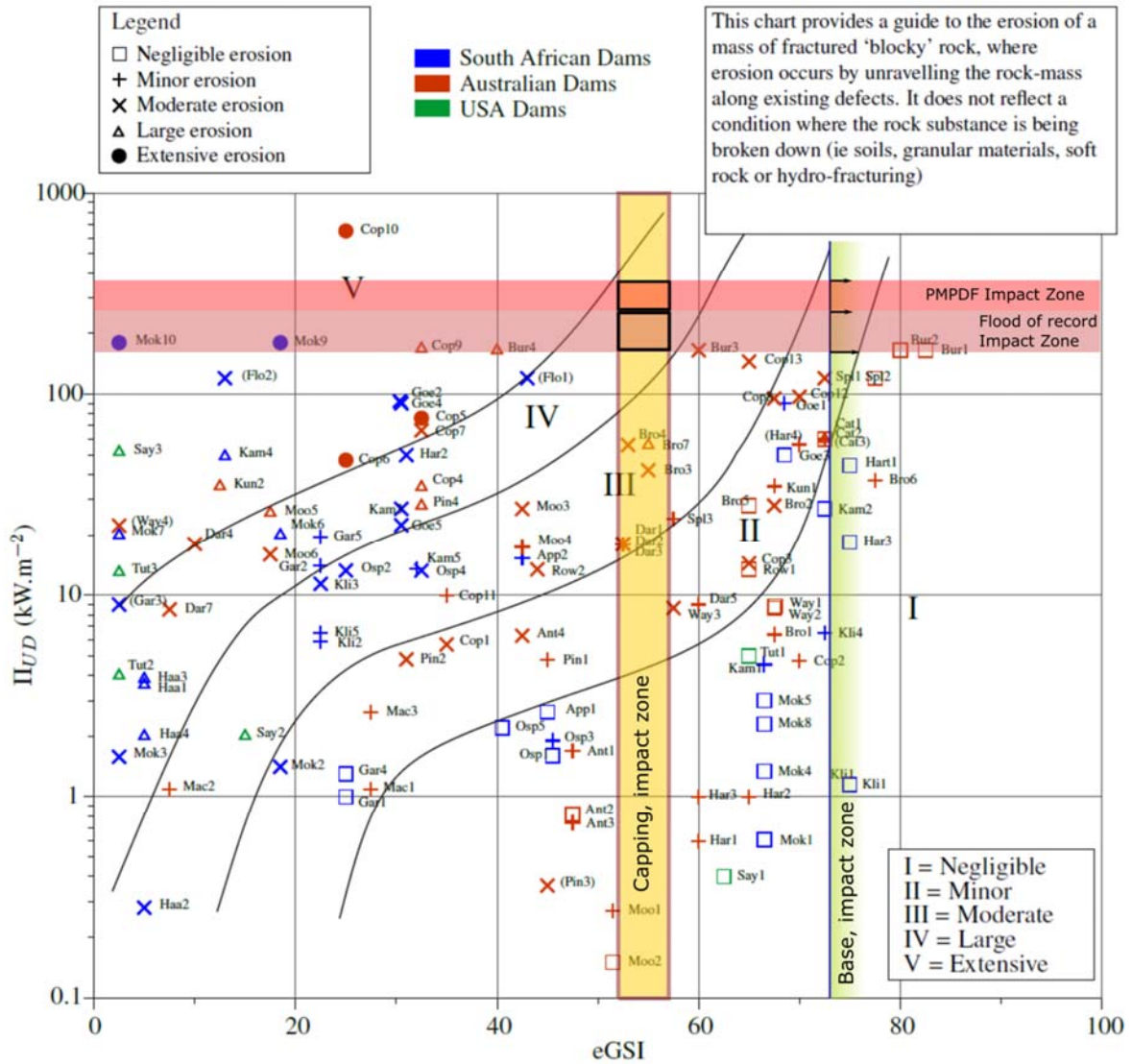


Figure 27 – eGSI erosion class, Impact Zone.



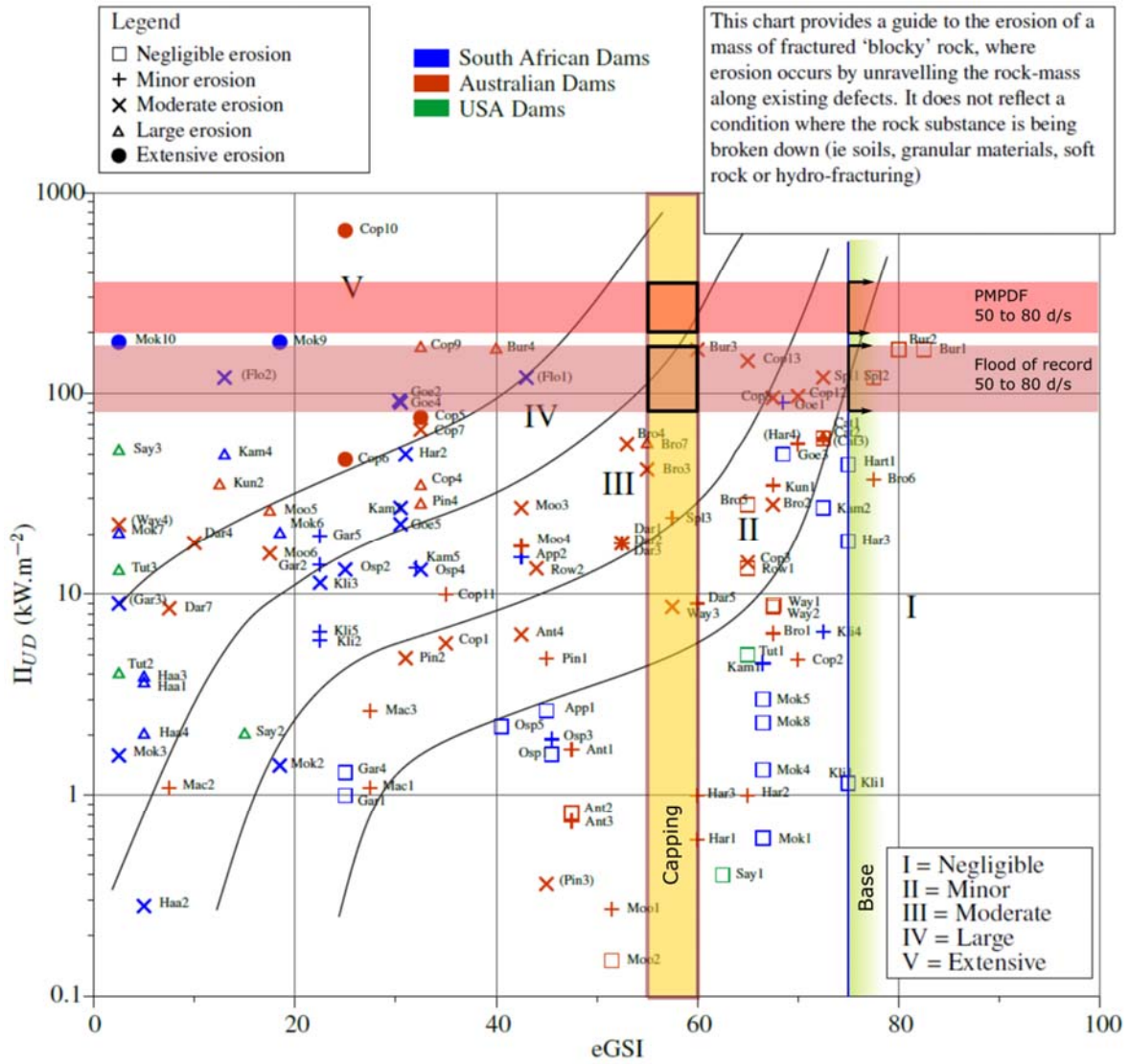


Figure 28 – eGSI erosion class, 50 to 80 d/s.

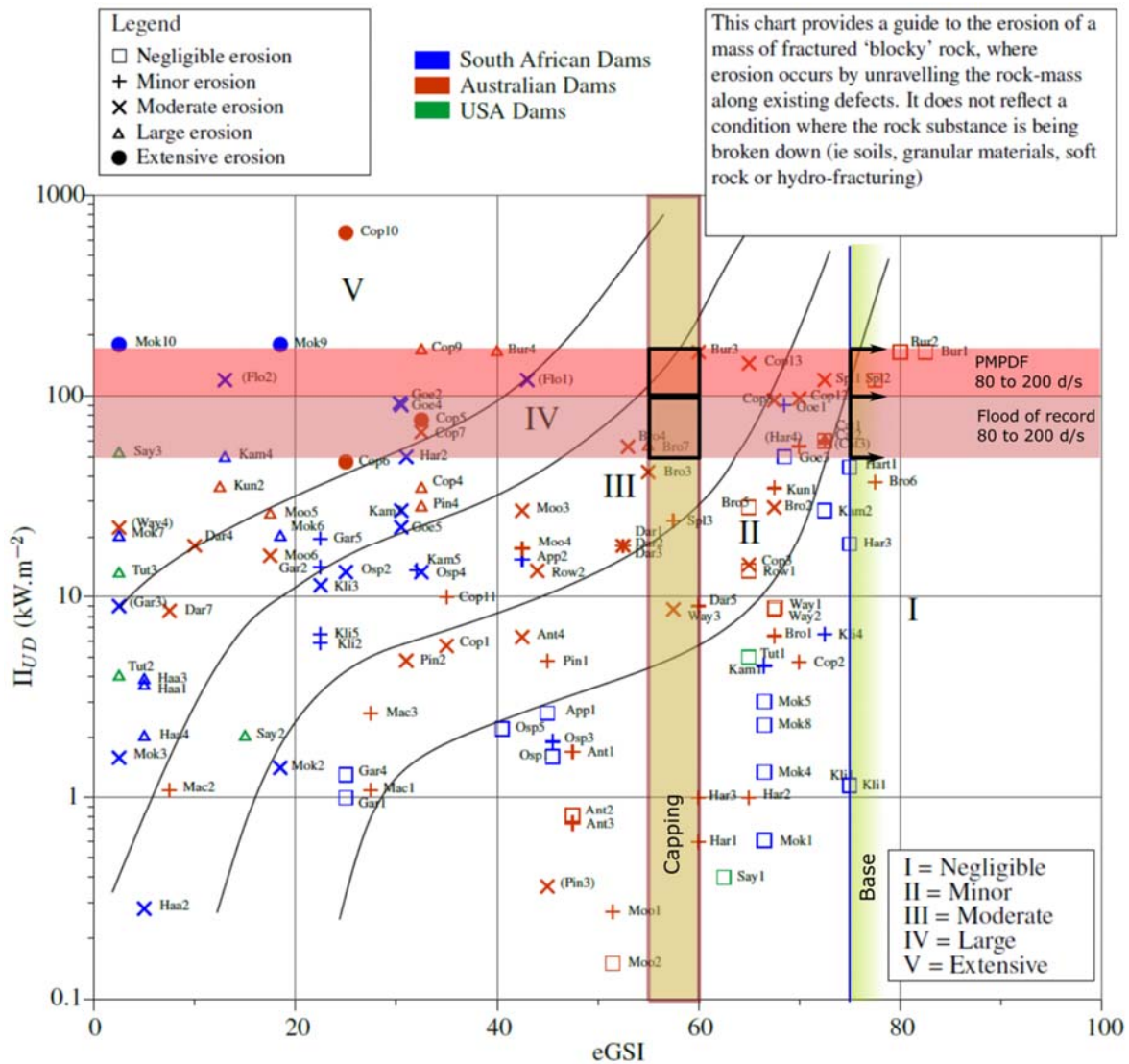


Figure 29 – eGSI erosion class, 80 to 200 d/s.

This assessment method indicates that “moderate” scour of capping material should be expected around the general spillway area during the PMPDF with “large” removal of capping within the plunge zone. Only minor to negligible scour of the base material is expected. The eGSI method indicates moderate to large quantities of capping material removed during the flood of record. Some areas appear to have conformed to this assessment, although perhaps not to the extent predicted.

RMEI values interpreted for the two geological domains are presented in Table 12, and the erosion classes determined from this analysis are shown in Table 13 (an example presentation of values on the RMEI chart is shown in Figure 30).

**Table 9 – Assessed RMEI values**

	Capping	Base
<b>P1</b>	3	1
<b>P2</b>	3	2
<b>P3</b>	2	1
<b>P4</b>	3	3
<b>P5</b>	3	2
<b>RMEI</b>	810	126

**Table 10 – Assessed RMEI erosion classes**

	Impact Zone		Transition (Jump) Zone 50 to 80 d/s		80 to 200 d/s	
	Capping	Base	Capping	Base	Capping	Base
Flood of record	III	I	III	I	II	I
PMPDF 1:9900 AEP	III	I	III	I	III	I

The RMEI method indicates slightly lower expectation of scour than the eGSI method. The base material is expected to resist scour, even under PMPDF flows, due to the assessed absence of kinematically viable mechanisms of removal. “Moderate” (30 to 100 m<sup>3</sup> per 100 m<sup>2</sup> area) removal of capping material is expected generally over the spillway domain, for events similar and larger than the flood of record.

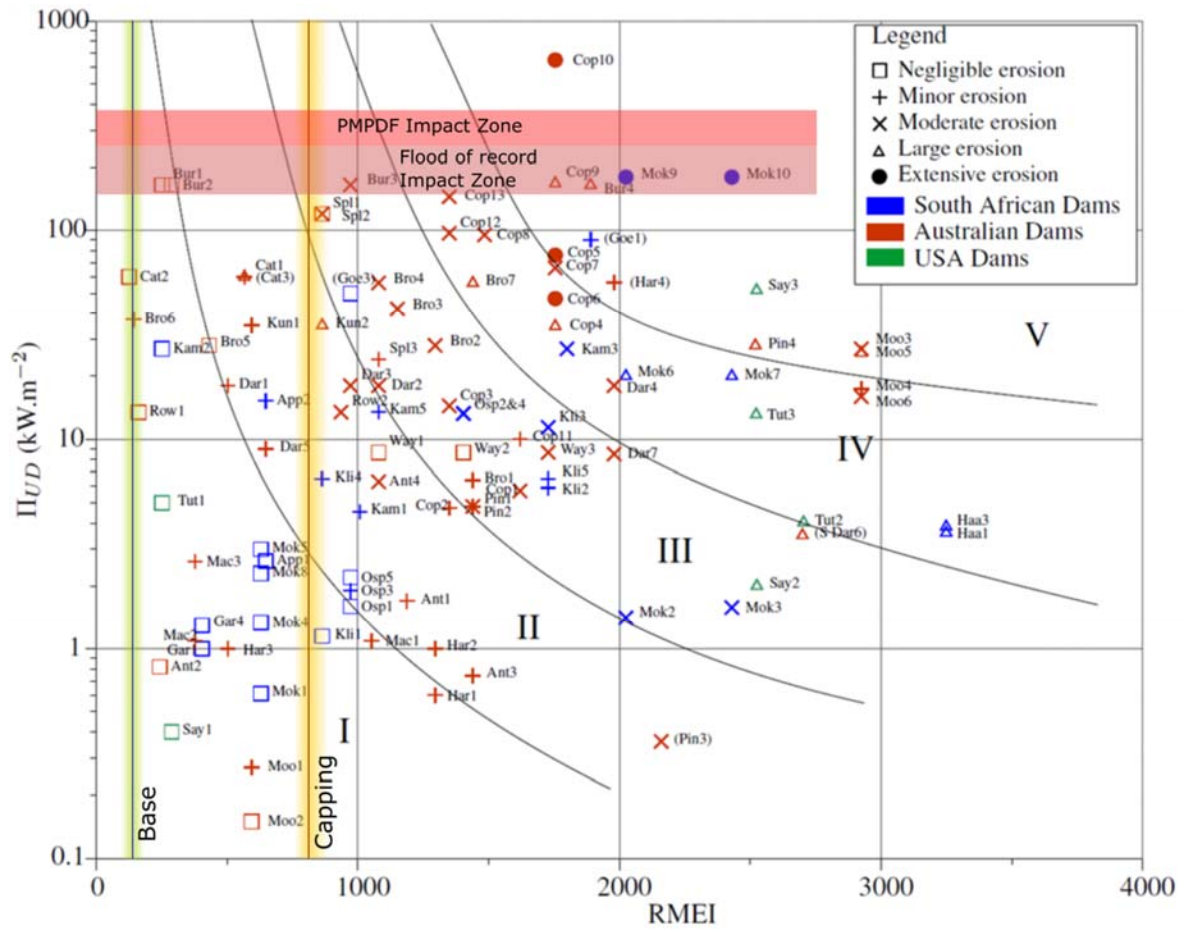


Figure 30 – RMEI erosion class, impact zone

## 5B. Analytical scour assessment

Within the discipline of rock mechanics, techniques are used to analytically assess the stability of rock slopes, tunnels or high-wall excavations. This involves resolving the force freebody for an identified rock (eg a 'key block') or particular section, and usually considers water pressures arising from seepage of groundwater. These types of analyses can be appropriated for examination of stability of spillways by incorporation of water pressures arising from spillway flows.

It is well known that the total energy embodied in a moving mass of water includes its kinetic and potential energy components. The kinetic component, due to its velocity ( $mu^2/2$ ) can be expressed as an equivalent potential form ( $mgh$ ), which can in turn be expressed as a pressure (in metres of head), yielding the well known expression of 'velocity head'  $h_u = u^2/2g$ . When a fluid is caused to slow down when impacting against a bluff object, the kinetic energy is transformed to a potential head or 'stagnation pressure' that acts against the object (referred to in literature as 'form drag'). Laboratory experiments (e.g. Reinus, 1986; Coleman *et al* 2003; Bollaert, 2003; Frizell, 2008; Pells 2016) have shown that stagnation of high velocity water against protrusions not only gives rise to locally high pressures, but that these pressures can be translated through adjacent rock defects, effectively penetrating into a rock mass. It has also been observed within these above cited experiments that turbulent fluctuations give rise to fluctuating pressures. It is the pressure differential between exposed and sheltered faces of a block of rock that give rise to the drag forces that are responsible for erosion. Techniques for estimation of these pressures are presented below.

### Design Coefficients

The proportion of the available velocity head that is translated into a stagnation pressure depends upon the geometry of the problem. Laboratory experiments have been undertaken to allow estimation of the proportion of velocity being converted to pressure head for various geometric conditions. This proportionality constant, denoted " $C_p$ " as observed in a test, can be expressed as:

$$C_{p_{\text{test}}} = \frac{P_{\text{test}}}{\rho g H_{\text{test}}} \quad (13)$$

Where  $P_{\text{test}}$  is the pressure (Pa) recorded during the experiment}

$H_{\text{test}}$  is some pressure head (m) characterizing the scale of the experiment

The conditions observed in the laboratory can be used to determine pressures at the prototype scale by reversing the equation:

$$P_{\text{prototype}} = C_{p_{\text{test}}} \rho g H_{\text{design}} \quad (14)$$

A problem is encountered in representing both the velocity head ' $h_v$ ' and the pressure head ' $h_p$ ' of the flow because, in practice, test  $C_p$  values are applied to real world conditions that are not

necessarily Froude scales of the test conditions - a single coefficient cannot represent both static and dynamic elements for all Froude conditions. This problem is resolved by assuming that the pressure head  $h_p$  in both test and design conditions, is hydrostatic and is therefore determinable in each case, and  $C_p$  values are derived with reference to velocity head only, and are applied, in design, to determine stagnation pressures only. Average pressure coefficients (denoted  $\overline{C_p}$ ) are thus assessed from laboratory experiments with the following expression:

$$\overline{C_p} = \frac{\overline{P}_{\text{test}} - h_p}{\overline{u}^2 / 2g} \quad (15)$$

where:  $\overline{P}_{\text{test}}$  = the mean pressure (Pa) recorded by a pressure transducer  
 $h_p$  = the static pressure head (m) at the observation point in the test  
(hydrostatic pressure normal to the slope assumed)  
 $\overline{u}$  = the time and depth averaged flow velocity

Design average pressure  $\overline{P}$  is thus calculated at a point on an element in any prototype by rearrangement of Equation 16:

$$\overline{P} = \overline{C_p} \rho \frac{\overline{u}^2}{2} + \rho g h_p \quad (16)$$

where:  $\overline{P}$  = the mean pressure (Pa) acting on the prototype  
 $h_p$  = the static pressure head (m) at the observation point in the prototype  
(hydrostatic pressure normal to the slope assumed)

This could also be expressed as

$$\overline{P} = \overline{P}_{\text{dyn}} + P_H \quad (17)$$

where:  $\overline{P}_{\text{dyn}}$  = the mean dynamic pressure (Pa) acting on the prototype  
 $P_H$  = the static pressure head (m)

Turbulence causes velocities to fluctuate, resulting in fluctuating stagnation pressures. It can be said that the total pressure ( $P$ ) at any time is the sum of mean ( $\overline{P}$ ) and fluctuating ( $P'$ ) components, ie:

$$P = \overline{P} + P' \quad (18)$$

Detailed analysis of laboratory measurements presented in Pells (2016a) demonstrated that the observed fluctuating pressures  $P'$  could be represented by a normal statistical distribution. The standard deviation of pressure fluctuations (denoted  $\sigma_p$ ) can be calculated at a point on an element as:

$$\sigma_p = C_{p,\sigma} \rho \frac{\bar{u}^2}{2} \quad (19)$$

where:  $C_{p,\sigma}$  = a fluctuating pressure coefficient (determined through experimentation)

As such, the probability of a certain total pressure  $P$  acting on a face at any time is assessed in accordance with a normal statistical distribution:

$$Prob(P) = \frac{1}{\sqrt{2\pi}\sigma_p} e^{-\frac{(P-\bar{P})^2}{2\sigma_p^2}} \quad (20)$$

Coefficients for a range of geometric and flow conditions were developed from detailed analysis of the test data presented in Pells (2016a), and are summarized in Tables 11 and 12. These pressure coefficients (Tables 12 and 13) can be used by a practitioner to estimate forces (or moments) on any element - the coefficients are distributed around the surface area of element in accordance with observations made, and the forces are determined by integrating the product of pressure and area to determine a principle force.

Coefficients of force (or moments) can be derived in a similar manner, allowing for forces to be determined directly, but these can be derived only for some idealised geometric conditions where the distribution of pressure in a particular test configuration is expected to be replicated in the prototype (real world). In Table 14, values for direct estimation of drag and lift forces, and moments, are presented based on testing of cubic blocks as presented in Pells (2016a).

Rock masses are complex materials and are unique to each site. It is not appropriate to develop a single 'black box' approach for generic analysis of stability of all unlined spillways. Rather, practitioners need to apply first principles physics to estimate a force freebody on a selected rock unit or section of slope. For example, each of the postulated mechanisms for the type section in Figure 31 could be assessed analytically.

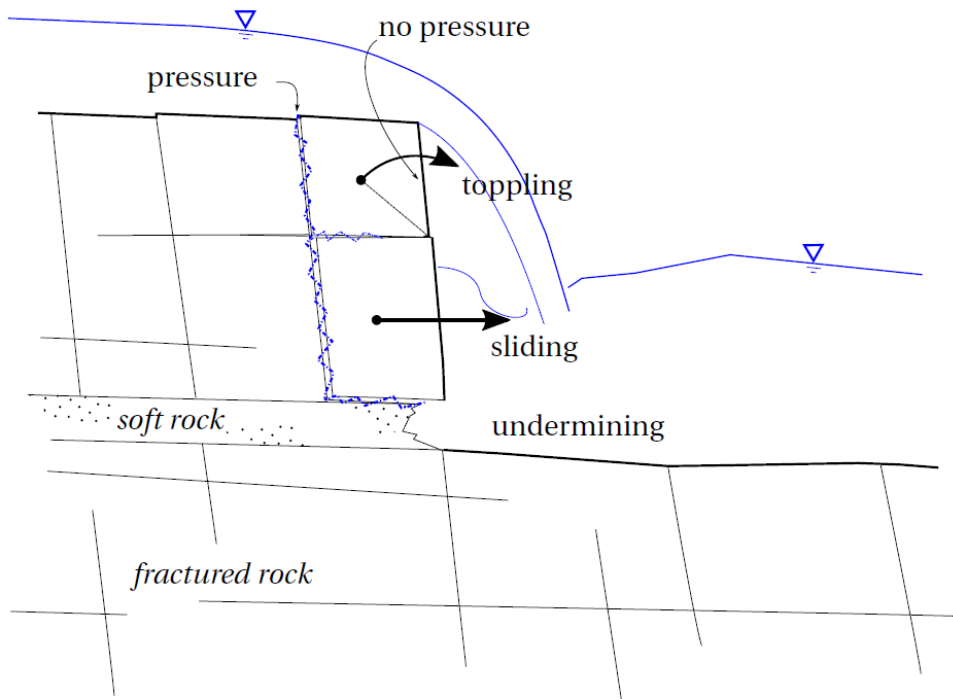


**Figure 31 – Postulated mechanisms for parallel retreat of headcuts in fractured rock**

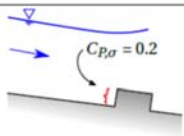
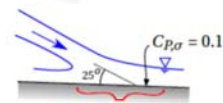
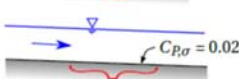
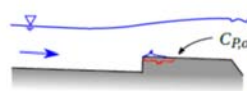
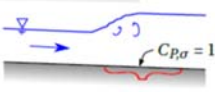
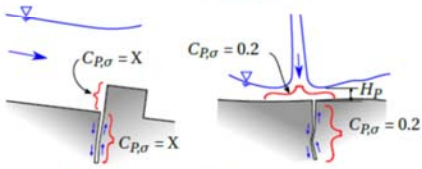
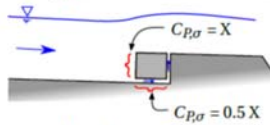
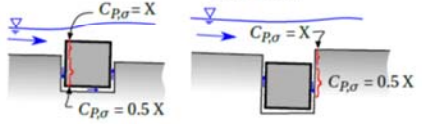
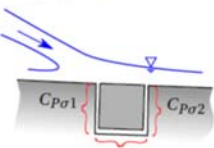
Where the average pressures on a rock are sufficient to cause detachment of a block, erosion of the rock mass could be said to occur rapidly. However, even where the mean pressures are insufficient to cause instability, erosion may occur under the action of pressure fluctuations that are higher than the average. Each fluctuation can be considered to cause a small movement, and hence a time-scale of erosion is inferred by considering the probability distribution function of pressure fluctuations. An example of such analysis is presented below.



Table 11 –  $C_p$  values for determination of mean pressures

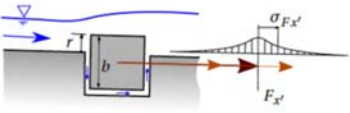
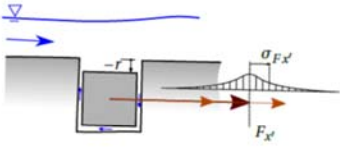
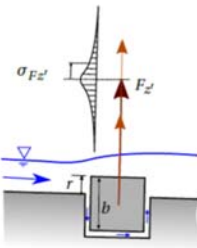
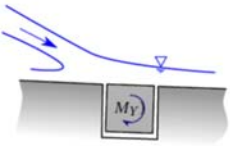
Hydraulic Action	Design Equation	Design coefficient	Examples
$\bar{P}$ (kPa)	$= \bar{C}_p \rho \frac{u^2}{2} + H_p \rho g$	<p><math>\bar{C}_p = 0.8</math> to 1 for surfaces protruding perpendicular to bed-parallel flow or jet impingement.</p> <p><math>\bar{C}_p = 0.2</math> for surfaces <math>25^\circ</math> to flow direction or jet impingement.</p> <p><math>\bar{C}_p = 0</math> to 0.1 for surfaces parallel (stream-lined) to flow, no detachment.</p> <p><math>\bar{C}_p = -\frac{H_p}{H_u}</math> (ie <math>\bar{P} = 0</math>) where flow fully detached from surface.</p> <p><math>\bar{C}_p = -2\frac{H_p}{H_u}</math> where flow detachment imminent.</p> <p>Daylighting, single-ended defects adopt the surface <math>\bar{C}_p</math> value.</p> <p>Daylighting, throughflowing, defects with dip parallel to impinging flow adopt the surface <math>\bar{C}_p</math> value.</p> <p>Daylighting, throughflowing, defects with dip perpendicular to impinging flow adopt <math>0.4 \times</math> surface <math>\bar{C}_p</math> value.</p> <p>Buried (ie - non-daylighting) defects adopt <math>0.75 \times</math> average of connected defect <math>\bar{C}_p</math> values.</p>	

Table 12 –  $C_p'$  values for determination of fluctuating pressures

Hydraulic Action	Design Equation	Design coefficient	Examples
$\sigma_p$ (kPa)	$= C_{p\sigma} \rho \frac{u^2}{2}$	$C_{p\sigma} = 0.2$ for surfaces protruding perpendicular to bed-parallel flow or jet impingement.#1.	
		$C_{p\sigma} = 0.1$ for surfaces 25° to flow direction or jet impingement. #1.	
		$C_{p\sigma} = 0.02$ for surfaces parallel (streamlined) to flow, no detachment.#1.	
		$C_{p\sigma} = 0.2$ where flow detachment imminent.	
		$C_{p\sigma} = 1$ for surfaces under an hydraulic jump	
		Daylighting, single-ended defects adopt the surface $C_{p\sigma}$ value.	
		Daylighting, thoughflowing, defects with dip parallel to impinging flow adopt 0.5 x surface $C_{p\sigma}$ value.	
		Daylighting, thoughflowing, defects with dip perpendicular to impinging flow adopt 0.5 x surface $C_{p\sigma}$ value.	
		Buried (ie - non-daylighting) defects adopt 0.75 x average of connected defect $C_{p\sigma}$ values.	
			$C_{p\sigma 3} = 0.75 \times \text{average}(C_{p\sigma 1}, C_{p\sigma 2})$

#1. Increase  $C_{p\sigma}$  values x 1.5 for self-aerated flows (Section ??).

Table 13 – Coefficients for determination of drag, lift and moments on cubic blocks

Hydraulic Action	Design Equation	Design coefficient	Examples
$F_x$ (N)	$= C_D \rho \frac{u^2}{2} r w$	$C_D = \frac{2}{3} \sqrt{\frac{D}{ r }}$ , or $= \frac{200}{R_{*s}^{0.5}}$ for bed-parallel flows and flows impinging at $\leq 20^\circ$ from bed slope	
or $F_x$ (N)	$= C_D \frac{\alpha}{2} \bar{\tau}_b b w \frac{ r-k_1 }{r-k_1}$	$C_D = 0.4$ for bed-parallel flows	
$\sigma_{Fx'}$	$= C_{D,\sigma} \rho \frac{u^2}{2} r w + C_{fd,\sigma} \rho \frac{u^2}{2} b w$	bed-parallel flows: $C_{D,\sigma} = 0.12 \sqrt{\frac{D}{ r }}$ ; $C_{fd,\sigma} = 0$ self-aerated bed-parallel flows: $C_{D,\sigma} = 0.24 \sqrt{\frac{D}{ r }}$ ; $C_{fd,\sigma} = 0$ flows impinging at mild angle: $C_{D,\sigma} = 0.12 \sqrt{\frac{D}{ r }}$ ; $C_{fd,\sigma} = 0.034$	
$F_z$ (N)	$= F_{sub} + F_L$ $= \nabla_{sub} \rho g + C_L \rho \frac{u^2}{2}  r  w$	$C_L = 0.9 \sqrt{\frac{D}{ r }}$ or $= \frac{200}{R_{*s}^{0.5}}$ for bed-parallel flows and flows impinging at $\leq 20^\circ$ from bed slope	
or $F_z$ (N)	$= F_{sub} + F_L$ $= \nabla_{sub} \rho g + C_L \frac{\alpha}{2} \bar{\tau}_b l w$	$C_L = 0.7$ for bed-parallel flows	
$\sigma_{Fz'}$	$= C_{L,\sigma} \rho \frac{u^2}{2} r w + C_{fl,\sigma} \rho \frac{u^2}{2} b w$	bed-parallel flows: $C_{L,\sigma} = 0.12 \sqrt{\frac{D}{ r }}$ ; $C_{fl,\sigma} = 0$ self-aerated bed-parallel flows: $C_{L,\sigma} = 0.24 \sqrt{\frac{D}{ r }}$ ; $C_{fl,\sigma} = 0$ flows impinging at $\leq 20^\circ$ from bed slope: $C_{L,\sigma} = 0.12 \sqrt{\frac{D}{ r }}$ ; $C_{fl,\sigma} = 0.08$	
$M_y$	$= F_L \frac{b}{4}$	for bed-parallel flows and flows impinging at $\leq 20^\circ$ from bed slope	
$\sigma_{My}$	$= \sigma_{Fx'} \frac{b}{2}$		

## Examples of analytical assessment of block dislodgement

Examination of ground survey data at Burdekin Falls Dam showed removal of some of the upper rock mass ("capping" – see section 3B above) had occurred. A close up of a selected section is shown in Figure 32 below, with annotations made to show the rock structure. The peak flood condition that occurred during this period was  $14500\text{m}^3\cdot\text{s}^{-1}$ .

Examination of this block removal suggests that a key block was unconstrained on the downstream face and on one side. Hence resistance for removal is primarily along the basal joint. An example of geometry of such a key block is shown in Figure 33.

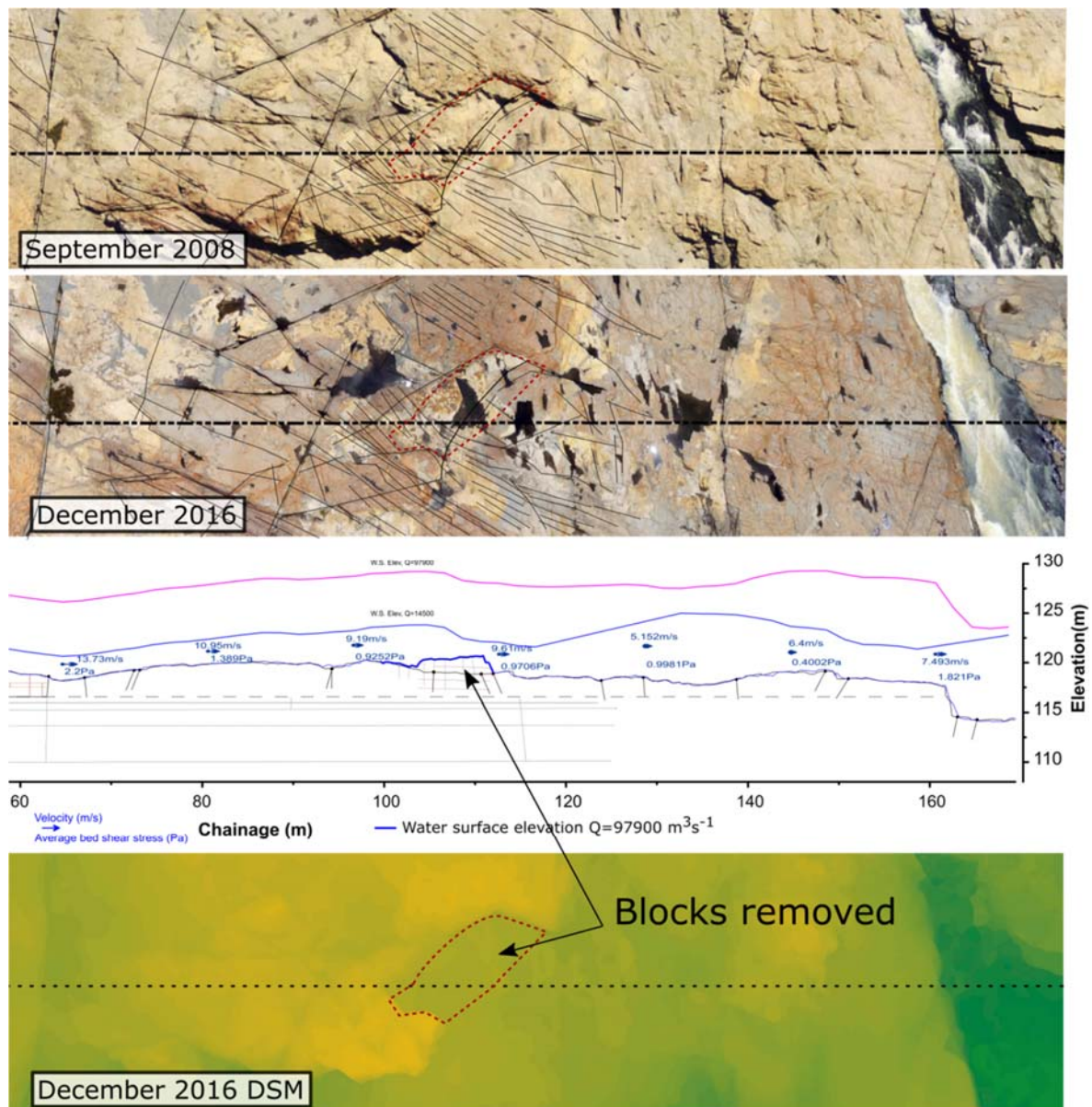


Figure 32 – Cross section along "Line C"

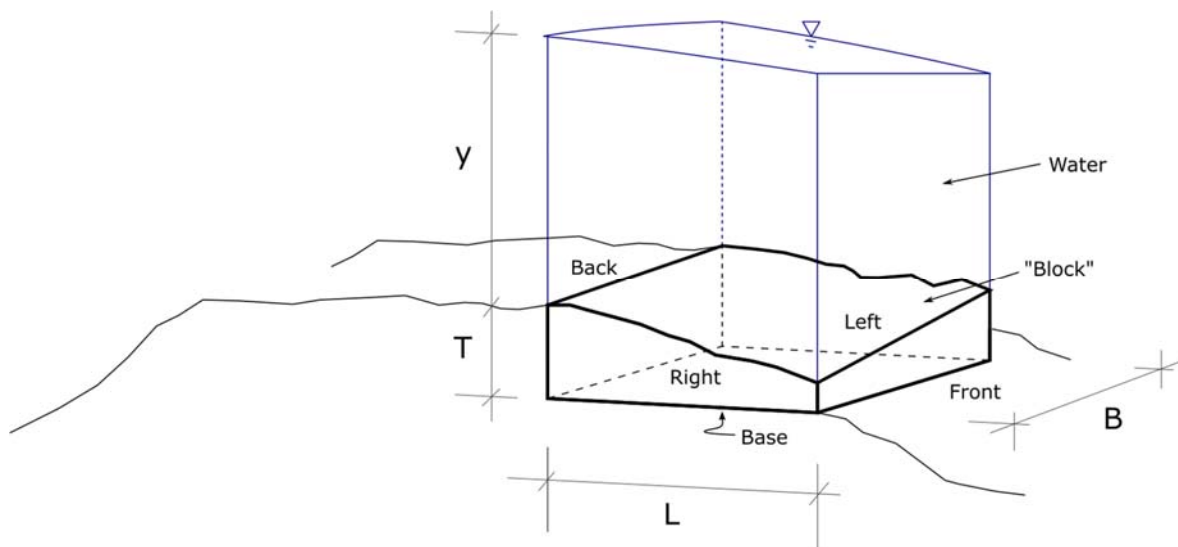


Figure 33 – Example of a key block on Line C

The pressures applied to the rock block shown in Figure 33 are presented below in Figure 34. Note that measurements presented in Pells (2016) indicated that dynamic pressure ( $\bar{C}_p$ ) along the basal joint can be estimated as being 75% of that along the upstream face, as shown.

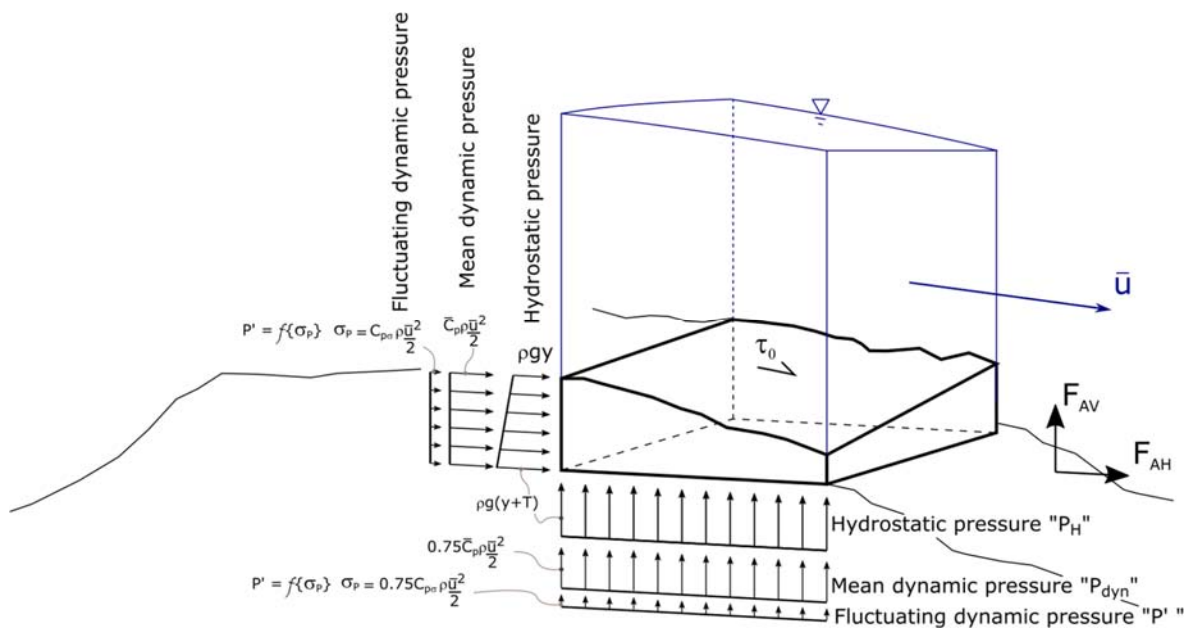


Figure 34– Hydraulic pressures applied to a block

Forces acting in a horizontal direction ( $F_{AH}$ ) can be expressed as (assuming hydrostatic only applies on upstream face<sup>3</sup>):

<sup>3</sup> i.e. assuming detachment of flow from the downstream face

$$F_{AH} = \tau_0 A_{top} + A_{front} \left[ \rho g y + \frac{\rho g T}{2} + \bar{C}_P \rho \frac{\bar{u}^2}{2} + P' \right]$$

$$F_{AH} \sim \tau_0 L B + \rho g T B \left[ y + \frac{T}{2} + \bar{C}_P \frac{\bar{u}^2}{2g} + \frac{P'}{\rho g} \right]$$

Forces acting in a vertical direction ( $F_{AV}$ ) can be expressed as:

$$F_{AV} = A_{base} \left[ \rho g (y + T) + 0.75 \bar{C}_P \rho \frac{\bar{u}^2}{2} + P' \right]$$

$$F_{AV} \sim \rho g L B \left[ y + T + 0.75 \bar{C}_P \frac{\bar{u}^2}{2g} + \frac{P'}{\rho g} \right]$$

Forces resisting movement are depicted in Figure 35.

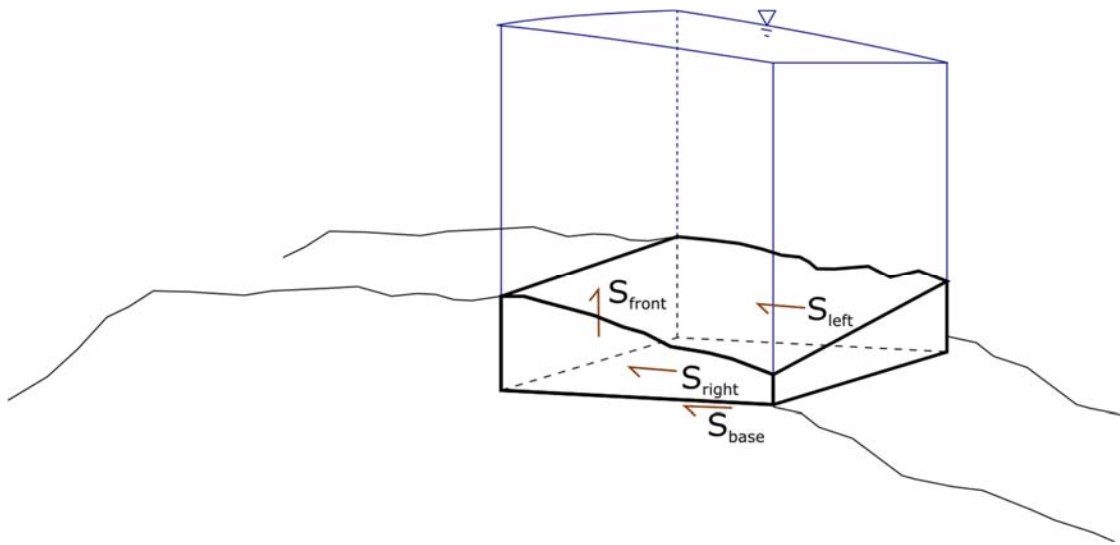


**Figure 35– Forces resisting movement of a block**

These shear forces 'S' can be estimated through principle of effective stress:

$$S = (N - pA) \tan \phi$$

Where:

$S$	=	a	shear	force	(Newton)
$N$	=	a	force	normal	to the shear plane (Newtons)
$p$	=	pore	pressures	along	the shear plane (Pascal)
$A$	=	area	of	the	shear plane (m <sup>2</sup> )
$\phi$	=	angle	of	friction	representing the rock mass defects (degrees)

For the resisting shear force along the base, for example, can be estimated as:

$$S_{base} = [\rho_R g \forall_R + \rho g \forall_W - F_{AV}] \tan \phi > 0$$

$$S_{base} = \left[ \rho_R g \forall_R + \rho g \forall_W - \rho g L B \left[ y + T + 0.75 \bar{C}_P \frac{\bar{u}^2}{2g} + \frac{P'}{\rho g} \right] \right] \tan \phi > 0$$

Where:  $\rho_R$  = density of the rock  
 $\forall_R$  = volume of the rock  
 $\forall_W$  = volume of water above the rock  
 $F_{AV}$  = hydraulic uplift force (presented above)

Assuming  $\forall_W \sim LBy$ , and  $\forall_R \sim LBT$  this reduces to:

$$S_{base} = \left[ \rho_R g L B T + \rho g L B y - \rho g L B \left[ y + T + 0.75 \bar{C}_P \frac{\bar{u}^2}{2g} + \frac{P'}{\rho g} \right] \right] \tan \phi > 0$$

$$S_{base} = \left[ T \left( \frac{\rho_R}{\rho} - 1 \right) - 0.75 \bar{C}_P \frac{\bar{u}^2}{2g} - \frac{P'}{\rho g} \right] \rho g L B \tan \phi > 0$$

(It is interesting to note that if  $\bar{C}_P > 0.47$  (ie 47% of the velocity head is translated into the basal joint), then the mean resisting force along the base becomes zero.)

At Burdekin Falls Dam, large shear forces along the left and right faces may exist along confined blocks due to the large insitu stress field. This would give rise to very large side shear resistances from blocks insitu. However, where one or more side faces are released, the insitu stress may be negated, resulting in a zero side shear force if the effective stress equation is applied. It has been observed at Burdekin Falls Dam that blocks are difficult to dislodge, even if one or more faces are released. The horizontal normal stress may be approximated either as: a 'cohesion' ' $\tau_R$ '. (ie  $S_{side} = \tau_R A_{side}$ ), or the side-normal force could be calculated as a proportion of the vertical or horizontal applied forces. A case where the side-normal force is taken as  $1/3^{rd}$  (an approximation using Poisson's ratio) of the vertical normal force is depicted in Figure 36.

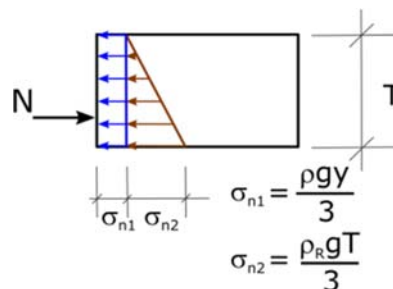


Figure 36– Option for representation of side-normal forces

In such a case, side resistance can be estimated as:

$$S_{left} = \left( \left[ \frac{\rho g y}{3} + \frac{\rho_R g T}{6} \right] - \left[ \rho g y + \frac{\rho g T}{2} + \bar{C}_P \rho \frac{\bar{u}^2}{2} + P' \right] \right) T L \tan \phi$$

$$S_{left} = \left( \left[ \frac{y}{3} + \frac{T \rho_R}{6 \rho} \right] - \left[ y + \frac{T}{2} + \bar{C}_P \frac{\bar{u}^2}{2g} + \frac{P'}{\rho g} \right] \right) \rho g T L \tan \phi$$

This equation indicates some side resistance when dry, but would result in reduced side forces once the block becomes submerged. Another alternative is to consider that side-shear force

becomes active as hydraulic forces seek to mobilise the block – i.e. the side-normal force is activated as a proportion 'C<sub>f</sub>' of the applied force - i.e:

$$S_{left} = \left( C_f \cdot F_{AV} - \left[ \rho g y + \frac{\rho g T}{2} + \bar{C}_p \rho \frac{\bar{u}^2}{2} + P' \right] TL \right) \tan \phi$$

$$S_{left} = \left( C_f \cdot B \left[ y + T + 0.75 \bar{C}_p \frac{\bar{u}^2}{2g} + \frac{P'}{\rho g} \right] - \left[ y + \frac{T}{2} + \bar{C}_p \frac{\bar{u}^2}{2g} + \frac{P'}{\rho g} \right] T \right) \rho g L \tan \phi$$

Movement of the block can be estimated when acting forces equal resisting forces, ie a factor of safety (FoS) = 1, where:

$$FoS = \frac{\text{resisting forces}}{\text{acting forces}}$$

For the case of sliding a FoS is therefore assessed as:

$$FoS_{slide} = \frac{S_{base} + S_{left}}{F_{AH}}$$

It can similarly be shown that, for overturning, the FOS is given by:

$$FoS_{OT} = \frac{\rho_R g \nabla_R \frac{L}{2} + \rho g \nabla_W \frac{L}{2} + S_{front} L}{F_{AV} \frac{L}{2} + F_{AH} \frac{T}{2}}$$

And for lifing:

$$FoS_{lift} = \frac{\rho_R g \nabla_R + \rho g \nabla_W + S_{left} + S_{front}}{F_{Av}}$$

Using the chosen dimensions (Figure 33), the following estimation for forces can be made (L=3, B=2, T=1, ρ<sub>R</sub>=2800 kg.m<sup>-3</sup>, φ = 45 degrees)

$$F_{AH} = 6\tau_0 + \rho g \left[ 2y + 1 + 2\bar{C}_p \frac{\bar{u}^2}{2g} + 2 \frac{P'}{\rho g} \right]$$

$$F_{AV} = \rho g \left[ 6y + 6 + 4.5\bar{C}_p \frac{\bar{u}^2}{2g} + 6 \frac{P'}{\rho g} \right]$$

$$S_{base} = \rho g \left[ 10.8 - 4.5\bar{C}_p \frac{\bar{u}^2}{2g} - 6 \frac{P'}{\rho g} \right] \geq 0$$

$$S_{left} = \rho g \left( 6(C_f - 0.25) + 6y(C_f - 0.5) + 4.5(C_f - 0.67)\bar{C}_p \frac{\bar{u}^2}{2g} + 6(C_f - 0.5) \frac{P'}{\rho g} \right) \geq 0$$

(or  $S_{left} = 3\tau_R$ )

For the case of the peak flood during the period wherein this block was removed, we have τ<sub>0</sub> ~1 kPa, y ~ 2.5 m,  $\bar{u}$  ~10 m.s<sup>-1</sup>. This gives (in kN):

$$F_{AH}(kN) = 65 + 100\bar{C}_p + 2P'$$

$$F_{AV}(kN) = 206 + 225\bar{C}_p + 6P'$$

$$S_{base}(kN) = 106 - 225\bar{C}_p - 6P' \geq 0$$



$$S_{left}(kN) = 206 (C_f - 0.43) + 225\bar{C}_p(C_f - 0.67) + 6(C_f - 0.5)P' \geq 0$$

Note that mean forces are represented for the case that  $P'=0$ . For example, the mean horizontal force ranges from 65 kN for  $\bar{C}_p = 0$  and ranges up to 160 kN for  $\bar{C}_p = 1$ . The mean lift force ranges from 206 kN for  $\bar{C}_p = 0$  and ranges up to 160 kN for  $\bar{C}_p = 1$ .

$\bar{C}_p$  and  $C_{p\sigma}$  values were examined in testing presented in Pells (2016).  $\bar{C}_p$  can be estimated as a function of protrusion ('r') of the exposed upstream face, as shown in **Figure 37**.

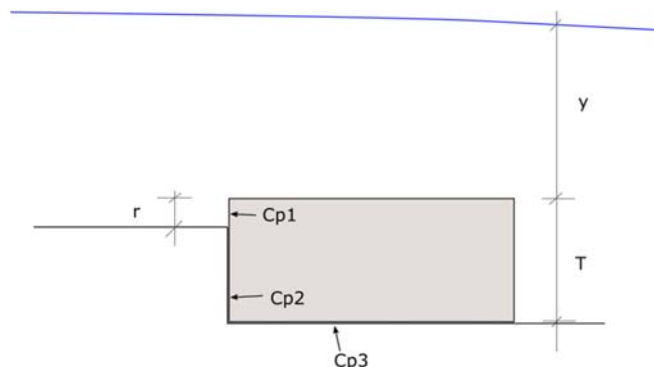


**Figure 37– Schematic showing various Cp values**

$$\bar{C}_{p1} \sim 2 \frac{r}{y} \quad \text{note } 0 < \bar{C}_p < 1$$

$$\bar{C}_{p2} \sim 0.8 \frac{r}{y} \quad \text{note } 0 < \bar{C}_p < 1$$

Therefore the average  $\bar{C}_p$  on the upstream face can be approximated as:

$$\bar{C}_p \sim 1.2 \frac{r}{y} \left( r + \frac{2}{3} \right) \quad \text{note } 0 < \bar{C}_p < 1$$

Note  $\bar{C}_{p3} \sim 0.75\bar{C}_p$ , which has been included in the above expressions of stability. The fluctuating pressure coefficient  $C_{p\sigma}$  was observed (Pells, 2016) to be  $\sim 0.2$  for exposed surfaces, and for defects connected to those surfaces. For the flood conditions being examined, this gives:

$$\sigma_p = 0.2 \rho \frac{\bar{u}^2}{2} = 10 \text{ kPa}$$

A range of conditions providing a FoS of unity for the cases of sliding, lifting and overturning are presented in Figure 38 as a function of  $\bar{C}_p$ . In Figure 39, this is reduced to a function of protrusion, using the equation for  $\bar{C}_p$  presented above.

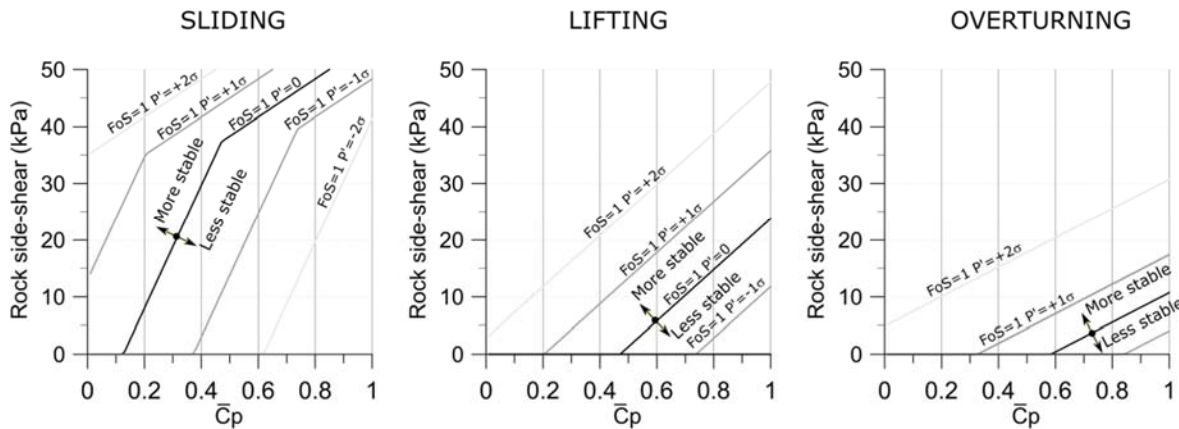


Figure 38– Rock side-shear and  $C_p$  values for FoS of unity

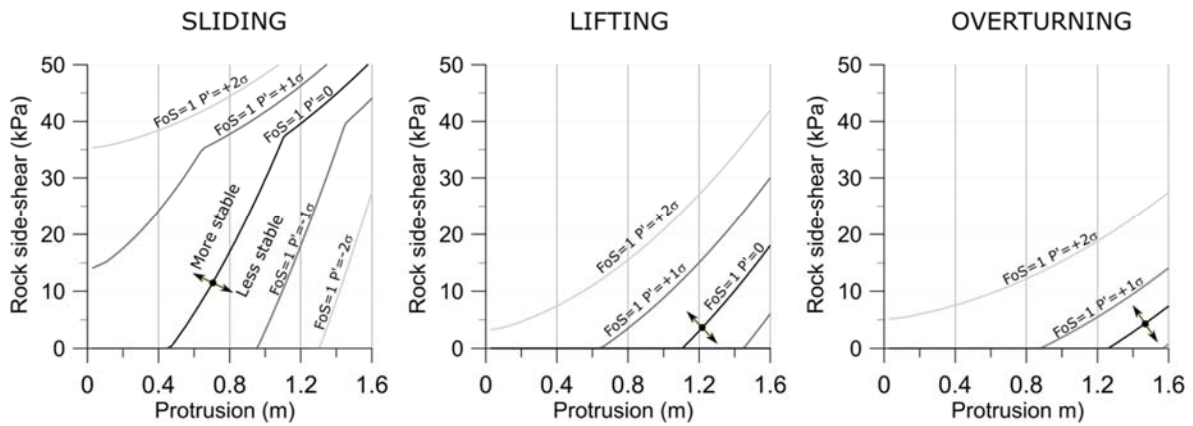


Figure 39– Rock side-shear and protrusion values for FoS of unity

The above calculations demonstrate various techniques of analytical assessment of stability with representation of pressure fluctuations by keeping the standard deviation of fluctuations as a design variable. Another alternative is to consider that the impulse imposed by each fluctuation causes an incremental movement of a selected block. Such a technique was demonstrated in Pells 2016, as applied to a selected block at Burdekin Falls Dam as shown in Figure 40. The result of this analysis in Figure 41 demonstrates how the time-scale of removal of rock units can be simulated analytically.

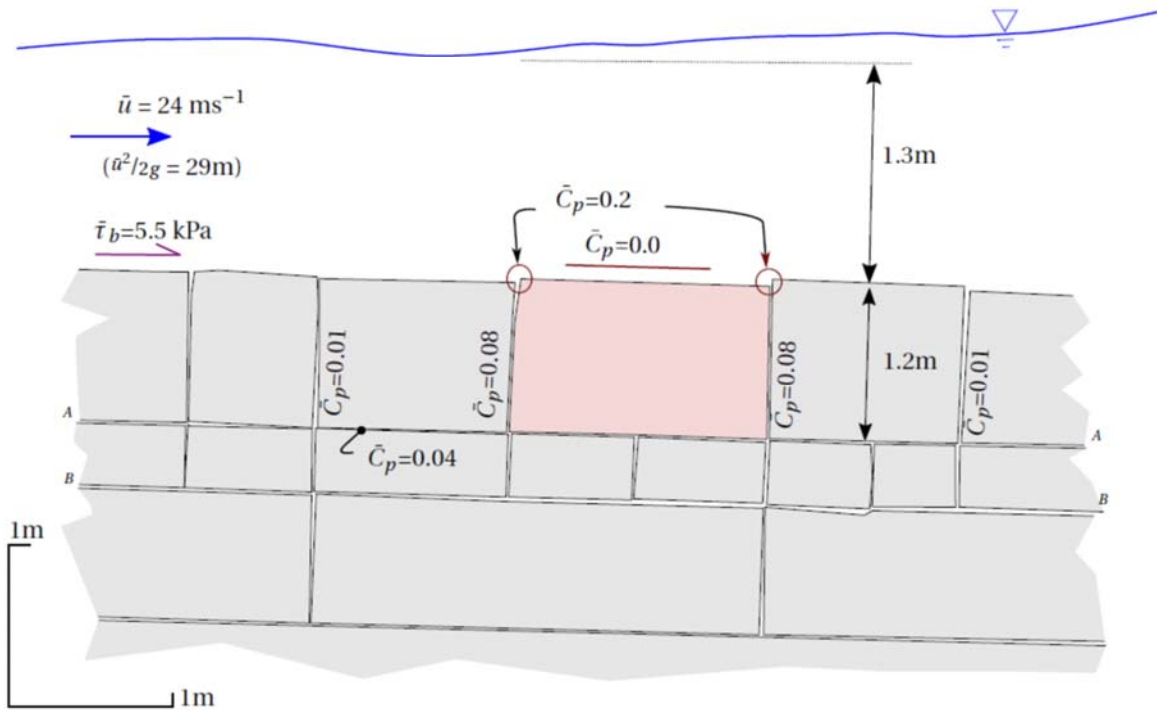


Figure 40 – Photograph and type-section at Burdekin Falls Dam

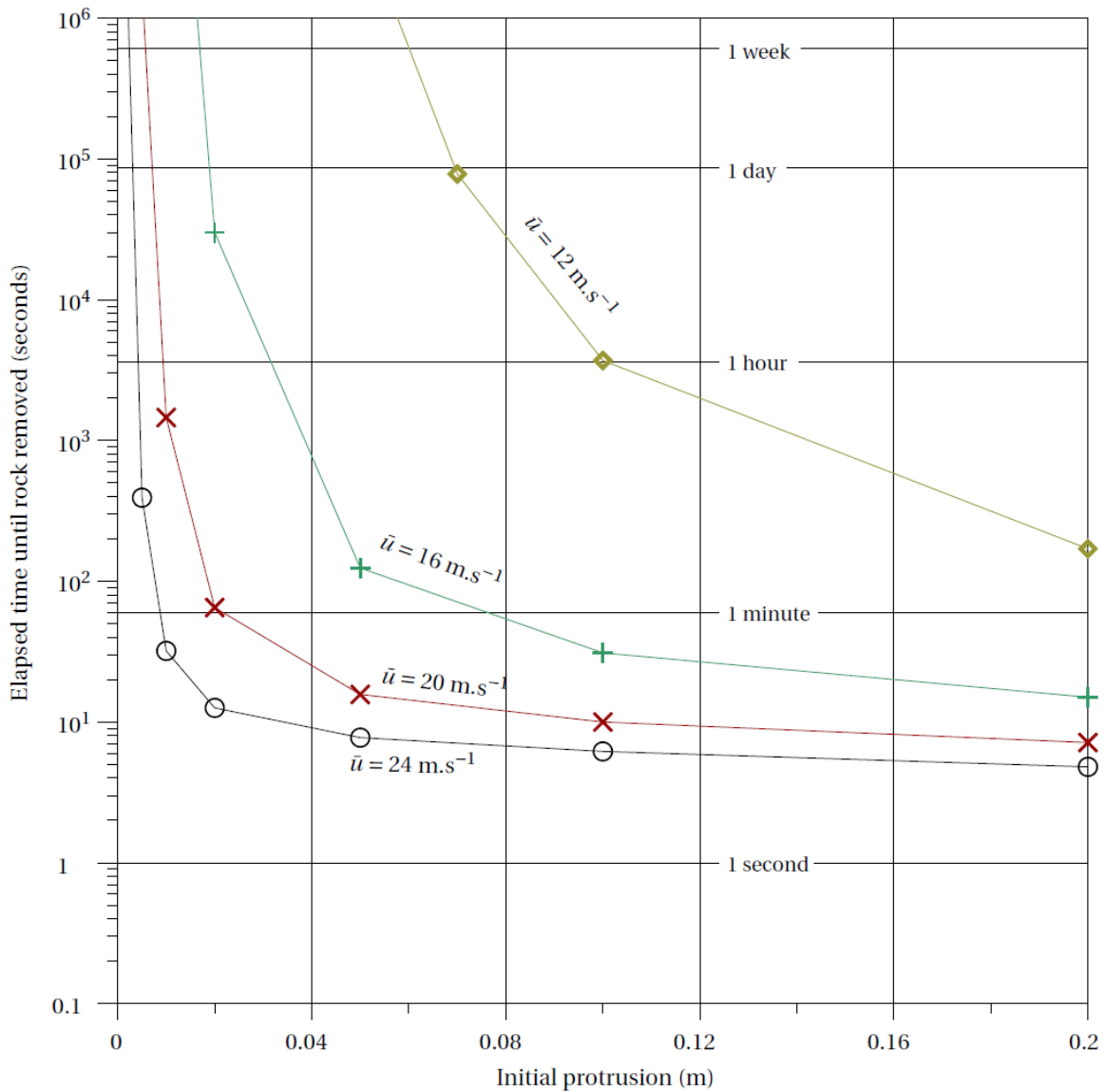


Figure 41 – Simulated time for entrainment of a block at Burdekin Falls Dam (from Pells, 2016)

From the above calculations, the following observations are made:

- Stability of a block at Burdekin Falls Dam is sensitive to the values of side-shear assumed. Values of over 20kPa are generally sufficient to provide resistance to movement of this block. It should be noted that if a block were constrained on both sides, and was subject to insitu stresses, the effective side-shear cohesion would be significantly larger (ie in MPa), ensuring stability against very large hydraulic forces.
- Stability of the block is also sensitive to the extent of sheltering or protrusion into the flow field. Where protrusion is very small, the rock has little vulnerability to being dislodged.
- Pressure fluctuations are significant to the stability of the block.

- Average bed shear stress provides a negligible contribution to hydraulic loading on the block.
- Analysis of smaller floods (not presented here) showed that the block was very unlikely to be dislodged during flows smaller than  $10000 \text{ m}^3 \cdot \text{s}^{-1}$ .

### **5C. Coupled numerical scour assessment**

The analytical methods presented above are somewhat arduous, and it falls upon the practitioner to perceive an appropriate section of the spillway, or representative key block, to analyze and to write and solve analytical equations as suitable. As shown in Section 3B above, current techniques of rock mass mapping and rock mass analysis can allow for detailed 3D models of rock masses. It follows then, that numerical analysis of erosion of rock masses can be achieved through coupled rock mass and hydrodynamic modelling.

At the time of writing, even advanced 3D computational fluid dynamic (CFD) models running on advanced computing platforms cannot practically simulate fluid dynamics at a resolution that would allow direct simulation of stagnation pressures on each individual protrusion over the spillway domain, nor the propagation of these pressures into each identified defect. At the current time, a practical way forward for such coupled modelling is to include a level of code which indirectly estimates stagnation pressures upon the rock mass from the flow depths and velocities determined from hydrodynamic models. Such an estimation would rely upon experimentally determined  $C_p$  values as applied in the analytical solutions presented in Section 5B above. The present writers know of no presently available commercial software package that does undertake this complete analysis. The dismantling of a 3D rock mass model can be achieved in various commercially available finite-element analysis software packages, and can be modified to incorporate hydraulic loading, taking outputs from hydrodynamic modelling. Results from CFD analysis are preferable for this application, as they provide spatially distributed results over the entire domain, and can utilize non-depth-averaged velocities for better examination of conditions close to the water-rock interface.

This type of analysis offers great promise for detailed examination of rock mass erosion but is an area requiring further development.

CFD models can output spatially-distributed estimations of  $\Pi_{UD}$  across the spillway domain. Such results can be used to guide definition of scour domains and comparative analysis using the techniques set out in Section 5B above. However, rock mass indices are not adequate representations of rock mass structures to support detailed coupled-process modelling of erosion.

## **6. Risk evaluation**

In dam engineering, risk is typically considered as the product of likelihood of occurrence and consequence. When undertaking the erosion assessment methods as set out above, the likelihood of occurrence is inferred by the return period associated with the flood conditions

that are assessed. The consequence of erosion is typically unique to each dam. In severe cases, the predicted erosion may lead to a dam breach. In other cases, the predicted erosion may incur expenses for repair. Risk from erosion should also consider the uncertainty in the prediction. All methods for erosion estimation presented above rely on interpretation. None of the methods provide a definitive assessment of scour extents. As such, following the analysis techniques set out above, an appropriately attended risk-assessment workshop should give thoughtful consideration to erosion mechanisms, prediction of erosion development and assessment of risk.

## **7. Assessment of protection measures**

Where the risks from erosion are unacceptable, solutions for mitigation will be considered. Pragmatically, the only solutions that exist are either to reduce the hydraulic loading, or to decrease the erodibility of a rock mass.

Clearly, hydraulic loading may be reduced by redirecting flow away from a region. After extensive erosion was observed at Copeton Dam (Australia), such a risk reduction approach was adopted by redirection of flow. A dividing wall was constructed (Figure 42) to isolate the more vulnerable region, designating it to be a secondary spillway. Redirection of flows may not always be feasible, and other methods of reducing hydraulic loading may be sought. Literature on spillway design includes various methodologies for energy dissipation, the opportunities for employing such techniques should be explored to manage erosion risk. The unit stream power dissipation ( $\Pi_{UD}$ ) is a function of flow width and, inasmuch as  $\Pi_{UD}$  is a suitable indicator of hydraulic loading, it is evident that distributing the flow over a larger area will reduce the erosive capacity of flow. The corollary is also true –the formation of flow gully's at Copeton Dam (Australia) and Mokolo Dam (South Africa – see Figure 43 and Figure 44) led to increasing  $\Pi_{UD}$  within the gully, which was postulated by Pells et al 2016 to be a major contributing factor to the extensive scour that occurred at these dams. The placement of concrete sills at the edge of the unlined steps in the spillway at Dartmouth Dam (Australia) (Figure 45) is also an illustration of flow spreading – this approach was found to be effective in ensuring that flows are evenly distributed over the step, avoiding further incision by erosion at low points.

Techniques to increase the erosion resistance of the rock mass may include concrete lining, dental concrete or rock-bolting. Illustrations of effective dental concrete are presented in Figure 46 (Copeton Dam) and Figure 47 (Pindari Dam). It could be argued that timely placement of dental concrete and / or a section of lining may have been sufficient to stop the formation of the large scour gully at Mokolo dam. Clearly, the placed concrete must itself be sufficient to resist hydraulic loads, and must also be of sufficient extent to avoid being undermined. Placement of concrete lining (Figure 48) within the deep scour gully at Copeton Dam was found, during test flows, to have insufficient extent to resist further headcutting.

Rockbolts can be effective in decreasing the erodibility of rock masses by locking together individual units to form an effectively larger intact mass. The rockbolt spacing should be commensurate with the block size. For example, rock bolts placed at Burdekin Falls Dam were

pattern placed with spacing larger than the block size, and were found to be ineffective at holding the blocks in place under hydraulic loading (Figure 49). Where closely spaced defects form smaller blocks, rock bolting may be tied into a surface mesh or surficial lining. It could also be argued that the unstressed rockbolts as installed at Burdekin Falls Dam are only effective once blocks are moving, and that stressed bolts may be more appropriate for the purposes of erosion resistance.

With reference to the structure of the flowchart in Figure 1, it is recommended that assessment of suitable protection measures is undertaken as part of the risk assessment process.

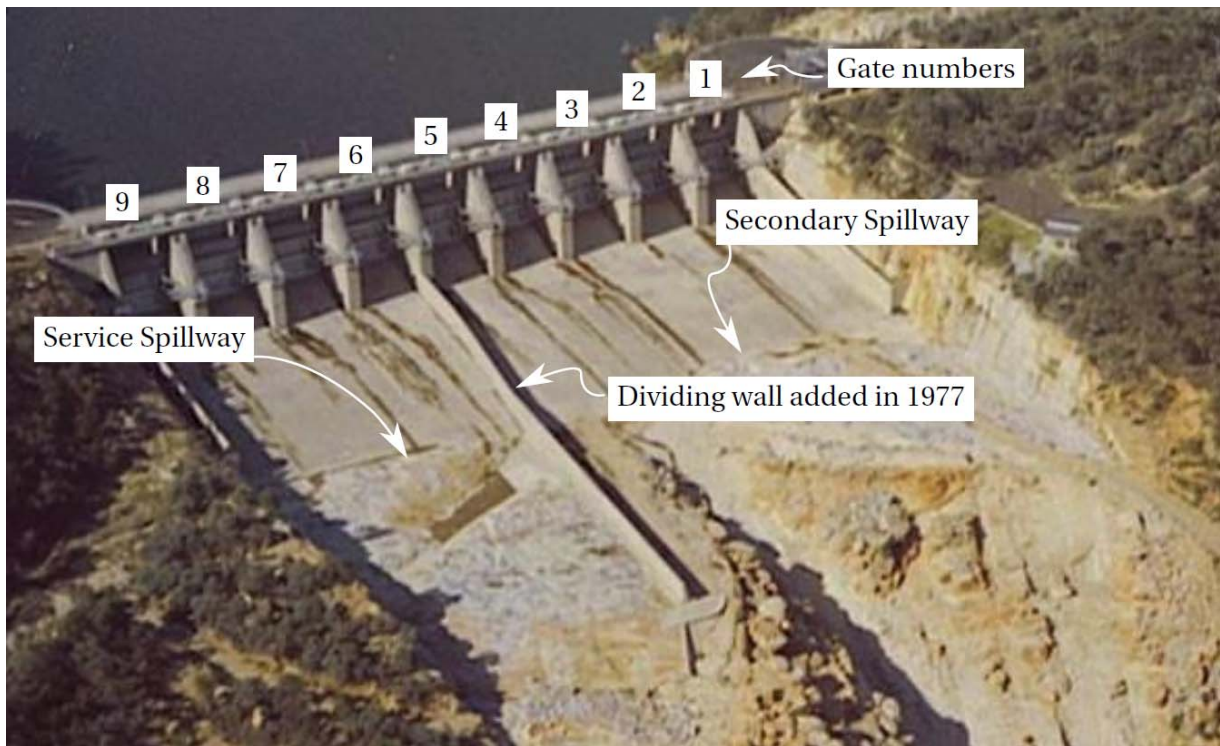


Figure 42 – An example of flow redirection to reduce erosion risk at Copeton Dam (Australia)



Figure 43 – Stream power dissipation was concentrated into a developed erosion channel at Mokolo Dam (South Africa, photo courtest of M. van Schalkwky).





Figure 44 – View of the large erosion channel at Mokolo Dam (South Africa, photo SE Pells)



Figure 45 – Placement of concrete sills to distribute flows over unlined cascades at Dartmouth Dam, preventing further channelisation



Figure 46 – A the void (see ponded region) formed after a wedge of rock was removed in the service spillway at Copeton Dam (NSW) was lined with concrete, which has proven effective



Figure 47 – Placement of dental concrete to fill a void left by erosion of blast-damaged rock at Pindari Dam (Australia) has proven effective



Figure 48 – Concrete lining placed within the erosion gully of the secondary spillway at Copeton Dam (Australia) was of insufficient extent to stop further headcutting occurring during test flows (photo SE Pells)



Figure 49 – The spacing for pattern bolting at Burdekin Falls Dam (Australia) exceeded the fracture frequency of ‘capping’ material, and was ineffective in stopping removal of individual rocks (photo courtesy of Sunwater)

## **8. Surveillance**

Surveillance should be undertaken following spill events. This is not only necessary to assess the significance of damage that may have occurred, but also provides some validation of the performance of the unlined spillway, against which the risk assessment can be compared.

The following procedure is recommended for surveillance of unlined spillways following significant spill events (from Pells 2016b):

1. Documentation of the spill event, including the time of peak reservoir levels and discharges.
2. A site walkover, attended by both engineering geologists and experienced hydraulics engineers. The walkover should formally document observed erosion (or lack thereof) using mapping and photographs.

3. The site inspection should be supported by detailed ground surveys. Techniques that allow rapid and cost effective 3D mapping of terrain which are now available and are recommended. Land or aircraft mounted LIDAR scanners can provide rapid and high accuracy surveys. Due to the lack of vegetation in spillways, very cost effective, and accurate 3D surveys can be undertaken by photogrammetry, using unmanned aerial vehicles (UAV's). An advantage of such photogrammetric surveys is also the provision of high-resolution aerial photographs, which can be used to map rock mass structure and for the preparation of 3D geological models. Comparison of 3D surveys before and after spill events can be used to prepare isopachs of erosion, which allow quick identification of erosion regions and patterns, as well as calculation of headcut advance and erosion volumes. Digital terrain models assembled from 3D surveys can also form the basis for rapid construction of revised spillway hydraulic models.
4. Where significant erosion that may modify flow characteristics has occurred, revised hydraulic analysis can be undertaken, providing synoptic profiles of hydraulic conditions throughout the spillway.
5. Where observed erosion does not reflect existing predictions, reassessment of rock mass erodibility, using the methods set out above, should be undertaken.
6. Based on the above information, the findings of previous risk-assessments should be reviewed, giving thoughtful consideration to observed erosion mechanisms, prediction of erosion development and assessment of risk.

In the experience of the present writers, a detailed review of erosion is often only undertaken after significant erosion has occurred so as to raise concerns for dam safety. In many of these cases, the effectiveness of the review was limited by the lack of suitable baseline data. In the case of Burdekin Falls Dam, the historical erosion in the spillway had been reported by some observers to be significant, warranting expensive protection measures, whereas other observers had reported that little or no erosion had occurred. These different reports had reflected differing perceptions of inspectors in the absence of factual data. The undertaking of cost effective UAV surveys provided an objective measurement of erosion that was able to resolve ongoing debates about how much erosion had historically occurred, and the perceived risk to further erosion. An inaccurate perception of erosion may similarly arise where incremental changes in spillway shape from sequential erosion events are each not perceived to be significant. For these reasons, dam owners / operators are urged to undertake routine spillway inspections, utilizing cost effective UAV survey techniques.

## **Summary and further research**

In this paper, guidelines for undertaking a "hydro-geotechnical rock scour assessment" are proposed, conforming to the flowchart presented in Figure 1. The proposed procedure uses current state-of-the-art techniques, which are illustrated with various examples. It is also recognized that ongoing research on this topic is active and is required. The proposed

methodology provides a framework that can readily include new techniques or advances as they become available.

From the methodology presented above, the following areas are identified as requiring research or development to improve the quality of rock mass erosion assessments:

1. Guidance on hydraulic roughness values (eg. Manning's  $n$  and absolute roughness  $k_s$ ) for high velocity, aerated flows over unlined spillways. This may be developed from prototype measurements / observations of spillway flows.
2. Further  $C_p$  values for ranging geometric conditions, including validation of the values presented herein against other laboratory tests, or against prototype measurements
3. Validated measurements and methods for analytical assessment of stream power dissipation for various rapidly varying flow conditions. The key unknown which requires further research is the rate of energy dissipation within features such as hydraulic jumps and plunging flows.
4. The comparative erosion assessment techniques presented herein were developed from observations of spillway erosion. In most cases, insufficient ground survey data was available for accurate characterization of the erosion extents. As UAV surveys become more commonplace, the comparative methods may be revised by inclusion of more accurate field observations. These methods will also benefit from improved hydrodynamic models run over the accurately surveyed surface, and with incorporation of improved methods for stream power dissipation assessment.
5. Development and validation of numerical simulation of rock mass scour using coupled 3D rock mass and hydrodynamics models.

## References

- Annandale, G.W., 1995. Erodibility. *Journal of hydraulic research* 33, 471–494.
- Bagnold, R.A. "An Approach to the Sediment Transport Problem from General Physics," U.S. Geological Survey Professional Paper 422-J, 1966, p.37
- Barton, N., Lien, R., and Lunde, J. (1974). "Engineering classification of rock masses for the design of tunnel support." *Rock Mech.*, 6(4), 189–236.
- Bieniawski, Z. T. (1973). "Engineering classification of jointed rock masses." *Civ. Eng. South Afr.*, 15(12), 335–344.
- Bertuzzi, R., Douglas, K., and Mostyn, G. (2016). "Comparison of quantified and chart GSI for four rock masses." *Eng. Geol.*, 202, 24–35.
- Coleman, S. E., Melville, B. W., and L. Gore. L (2003): "Fluvial Entrainment of Protruding Fractured Rock," *Journal of Hydraulic Engineering*, 129, 872–884.
- Dooge, N., 1993. Die hidrouliese erodeerbaarheid van rotmassas in onbelynde oorlope met spesiale verwysing na die rol van naatvulmateriaal (M.Sc Thesis). University of Pretoria, South Africa.

- Douglas K; Pells S; Fell R; Peirson W, 2018, 'The influence of geological conditions on erosion of unlined spillways in rock', *Quarterly Journal of Engineering Geology and Hydrogeology*, vol. 51, pp. 219 - 228, <http://dx.doi.org/10.1144/qjegh2017-087>
- Fell, R., M. Foster, J. Cyganiewicz, G. SILLS, N. Vroman, and R. Davidson (2008): "A unified method for estimating probabilities of failure of embankment dams by internal erosion and piping," Tech. Rep. UNICIV Report No. R 446, School of Civil and Environmental Engineering, UNSW Australia, Sydney.
- Frizell, K. W. (2008): Uplift and crack flow resulting from high velocity discharges over open offset joints: laboratory studies, Denver, Colo.: U.S. Dept. of the Interior, Bureau of Reclamation, Technical Service Center.
- Henderson, F. M. (1966). *Open channel flow*. New York, Macmillan.
- Hoek, E., Kaiser, P. K., and Bawden, W. F. (1995). Support of underground excavations in hard rock, A.A. Balkema, Rotterdam, Netherlands.
- Hudson, J. A., and Harrison, J. P. (2005). Engineering rock mechanics: An introduction to the principles, Pergamon, Tarrytown, NY.
- Kirsten, H., Kirsten, L., Kirsten, A., 1995. General classification system for hydraulic erosion (No. 197083/1). Steffen Robertson and Kirsten, Johannesburg.
- Kirsten, H. (1995). "Erodibility criterion for jet cutting of intact materials." Rep. 197083/3, Steffen, Robertson, and Kirsten Incorporated, Johannesburg, South Africa.
- Kirsten, H.A.D., 1982. Classification system for excavation in natural materials, in: Civil Engineer in South Africa. pp. 293–308.
- Kirsten, H.A.D., Moore, J.S., Kirsten, L.H., Temple, D.M., 2000. Erodibility criterion for auxiliary spillways of dams. *International Journal of Sediment Research* 15, 93–107.
- Moore, J.S., Kirsten, H., 1988. Discussion - Critique of the rock material classification procedure, in: Kirkaldie, L. (Editor), *Proceedings. Presented at the Rock Classification Systems for Engineering Purposes*, American Society for Testing and Materials, Philadelphia, pp. pp55-88.
- Moore, J. (1991). *The characterization of rock for hydraulic erodibility*, Water Resources Publications, Littleton, CO.
- Marinos, P., Hoek, E., 2000. GSI - A geologically friendly tool for rock mass strength estimation, in: *Proceedings. Presented at the GeoEng Conference*, Melbourne, pp. 1422–1442.
- Pells, S.E., 2016a. *Erosion of Rock in Spillways (Doctoral Thesis)*. UNSW Australia, Kensington, N.S.W.
- Pells, S.E. 2016b "Assessment and surveillance of erosion risk in unlined spillways" *International Symposium on "Appropriate technology to ensure proper Development, Operation and Maintenance of Dams in Developing Countries"*, Johannesburg, South Africa, 18 May 2016 © SANCOLD, ISBN 978-0-620-71042-8
- Pells S; Douglas K; Pells PJ N; Fell R; Peirson WL, 2016, 'Rock Mass Erodibility', *Journal of Hydraulic Engineering*, pp. 06016031 - 06016031, [http://dx.doi.org/10.1061/\(ASCE\)HY.1943-7900.0001243](http://dx.doi.org/10.1061/(ASCE)HY.1943-7900.0001243)
- Pells, P.J. Bieniawski, Z.T., Hencher, S.R., Pells, S.E. 2017 Rock quality designation (RQD): time to rest in peace. *Canadian Geotechnical Journal*, 2017, 54(6): 825-34, <https://doi.org/10.1139/cgj-2016-0012>
- Pitsiou, S., 1990. The effect of discontinuities on the erodibility of rock in unlined spillways (M.Sc Thesis). University of Pretoria, South Africa.
- van Schalkwyk, A., 1994. Minutes - Erosion of Rock in Unlined Spillways. ICOLD q.71 r.37, 1056–1062.

van Schalkwyk, A., Jordaan, J.M., Dooge, N., 1994a. Die erodeerbaarheid van verskillende rotsformasies onder varierende vloeitoestande (No. WNK Verslag No. 302/1/95). verslag aan die waternavorsingskommissie deur die Departement of Geologie, Universiteit van Pretoria, South Africa.

van Schalkwyk, A., Jordaan, J.M., Dooge, N., 1994b. Erosion of Rock in Unlined Spillways. International Commission on Large Dams Paris. Q.71 E.37, 555-571.